



## Original article

# Single-cell analyses reveal cannabidiol rewires tumor microenvironment via inhibiting alternative activation of macrophage and synergizes with anti-PD-1 in colon cancer

Xiaofan Sun <sup>a, b, 1</sup>, Lisha Zhou <sup>b, 1</sup>, Yi Wang <sup>c, 1</sup>, Guoliang Deng <sup>b</sup>, Xinran Cao <sup>b</sup>, Bowen Ke <sup>d</sup>, Xiaoqi Wu <sup>e</sup>, Yanhong Gu <sup>f</sup>, Haibo Cheng <sup>g</sup>, Qiang Xu <sup>b</sup>, Qianming Du <sup>h, i, \*\*\*</sup>, Hongqi Chen <sup>j, \*\*</sup>, Yang Sun <sup>a, b, k, \*</sup>

<sup>a</sup> Department of Rheumatology and Immunology, Nanjing Drum Tower Hospital, The Affiliated Hospital of Nanjing University Medical School, Nanjing University, Nanjing, 210008, China

<sup>b</sup> State Key Laboratory of Pharmaceutical Biotechnology, School of Life Sciences, Nanjing University, Nanjing, 210023, China

<sup>c</sup> Colon and Rectal Surgery, Nanjing Hospital of Chinese Medicine Affiliated to Nanjing University of Chinese Medicine, Nanjing, 210001, China

<sup>d</sup> Laboratory of Anesthesia and Critical Care Medicine, Department of Anesthesiology, Translational Neuroscience Center, West China Hospital and State Key Laboratory of Biotherapy, Sichuan University, Chengdu, 610044, China

<sup>e</sup> Genergy Bio-technology (Shanghai) Co., Ltd, Shanghai, 200241, China

<sup>f</sup> The First Affiliated Hospital of Nanjing Medical University, Jiangsu Province Hospital, Nanjing, 210029, China

<sup>g</sup> Jiangsu Collaborative Innovation Center of Traditional Chinese Medicine in Prevention and Treatment of Tumor, The First Clinical College of Nanjing University of Chinese Medicine, Nanjing, 210023, China

<sup>h</sup> General Clinical Research Center, Nanjing First Hospital, Nanjing Medical University, Nanjing, 210006, China

<sup>i</sup> School of Basic Medicine & Clinical Pharmacy, China Pharmaceutical University, Nanjing, 210009, China

<sup>j</sup> Department of General Surgery, Shanghai Jiao Tong University Affiliated Sixth People's Hospital, Shanghai, 200030, China

<sup>k</sup> Jiangsu Key Laboratory of New Drug Research and Clinical Pharmacy, Xuzhou Medical University, Xuzhou, Jiangsu, 221004, China

## ARTICLE INFO

## Article history:

Received 19 December 2022

Received in revised form

12 April 2023

Accepted 18 April 2023

Available online 22 April 2023

## Keywords:

scRNA-seq

scATAC-seq

Cannabidiol

Colorectal cancer

Tumor microenvironment

Macrophage

## ABSTRACT

Colorectal tumors often create an immunosuppressive microenvironment that prevents them from responding to immunotherapy. Cannabidiol (CBD) is a non-psychoactive natural active ingredient from the cannabis plant that has various pharmacological effects, including neuroprotective, antiemetic, anti-inflammatory, and antineoplastic activities. This study aimed to elucidate the specific anticancer mechanism of CBD by single-cell RNA sequencing (scRNA-seq) and single-cell ATAC sequencing (scATAC-seq) technologies. Here, we report that CBD inhibits colorectal cancer progression by modulating the suppressive tumor microenvironment (TME). Our single-cell transcriptome and ATAC sequencing results showed that CBD suppressed M2-like macrophages and promoted M1-like macrophages in tumors both in strength and quantity. Furthermore, CBD significantly enhanced the interaction between M1-like macrophages and tumor cells and restored the intrinsic anti-tumor properties of macrophages, thereby preventing tumor progression. Mechanistically, CBD altered the metabolic pattern of macrophages and related anti-tumor signaling pathways. We found that CBD inhibited the alternative activation of macrophages and shifted the metabolic process from oxidative phosphorylation and fatty acid oxidation to glycolysis by inhibiting the phosphatidylinositol 3-kinase-protein kinase B signaling pathway and related downstream target genes. Furthermore, CBD-mediated macrophage plasticity enhanced the response to anti-programmed cell death protein-1 (PD-1) immunotherapy in xenografted mice. Taken together, we provide new insights into the anti-tumor effects of CBD.

© 2023 The Author(s). Published by Elsevier B.V. on behalf of Xi'an Jiaotong University. This is an open access article under the CC BY-NC-ND license (<http://creativecommons.org/licenses/by-nc-nd/4.0/>).

Peer review under responsibility of Xi'an Jiaotong University.

\* Corresponding author. Department of Rheumatology and Immunology, Nanjing Drum Tower Hospital, The Affiliated Hospital of Nanjing University Medical School, Nanjing University, Nanjing, 210008, China.

\*\* Corresponding author.

\*\*\* Corresponding author. General Clinical Research Center, Nanjing First Hospital, Nanjing Medical University, Nanjing, 210006, China.

E-mail addresses: [duqianming@njmu.edu.cn](mailto:duqianming@njmu.edu.cn) (Q. Du), [hqchen08@163.com](mailto:hqchen08@163.com) (H. Chen), [yangsun@nju.edu.cn](mailto:yangsun@nju.edu.cn) (Y. Sun).

<sup>1</sup> These authors contributed equally to this work.

<https://doi.org/10.1016/j.jpha.2023.04.013>

2095-1779/© 2023 The Author(s). Published by Elsevier B.V. on behalf of Xi'an Jiaotong University. This is an open access article under the CC BY-NC-ND license (<http://creativecommons.org/licenses/by-nc-nd/4.0/>).

## 1. Introduction

Colorectal cancer (CRC), a malignant epithelial tumor, is the third most common cancer type and the second leading cause of cancer death. With the advent of more effective therapeutic approaches, especially immunotherapies, the prognosis of patients has significantly improved over the past 20 years [1,2]. Cancer immunotherapy has achieved a revolution in cancer treatment, including checkpoint inhibitors and adoptive cell therapy that manipulate the immune system to recognize and attack cancerous cells. However, despite the clinical success of immunotherapies such as antibodies against cytotoxic T lymphocyte antigen-4, programmed cell death protein 1 (PD-1), and its ligand PD-L1, and chimeric antigen receptors T cell therapy, only a subset of patients have responded fully to immunotherapy; the reasons for this are, as yet, unknown [3,4]. Thus, further insight into immunotherapy mechanisms as well as identification of novel therapies for CRC are urgently required.

Studies have shown that without coordinated strategies to mitigate the immunosuppressive properties of the tumor microenvironment (TME), cancer immunotherapies often provide limited clinical benefit [5–7]. As the predominant immunosuppressive component of the TME, tumor-associated macrophages (TAMs) play critical roles in tumor angiogenesis, tumor progression and metastasis, immunosuppression, resistance to chemotherapeutic agents, and checkpoint blockade immunotherapy [8,9]. Although macrophages can be characterized simply as classically activated pro-inflammatory (M1) macrophages or alternatively activated pro-tumorigenic (M2) macrophages, accumulated evidence suggests that macrophages in tumors display pro-tumorigenic M2 phenotypes for supporting tumor progression in the TME [10]. Cytokines in the TME, such as interleukin-4 (IL-4) and IL-13, drive macrophages into an alternatively activated state and alter the cellular metabolic state to rely on oxidative phosphorylation (OXPHOS) and fatty acid oxidation (FAO). Such shifts in cellular metabolic status in turn support the transcriptional activation of associated genes [11–14]. However, how metabolic reprogramming is orchestrated and which cellular and environmental signals are sensed to control the activation and polarization of macrophages remains unclear [15,16].

Cannabidiol (CBD), a non-psychoactive natural active ingredient from the cannabis plant, has various pharmacological effects including neuroprotective [17], anti-emetic [18], anti-inflammatory [19,20], and anti-tumor activities [21,22]. It has already been approved for the treatment of epilepsy in children by the U.S. Food and Drug Administration in 2018. In contrast to the psychoactive constituent tetrahydrocannabinol (THC), CBD has a low affinity to the cannabinoid receptors CB1 and CB2 [23,24]. Several studies have shown that CBD presents a strong anti-tumor ability [25], yet the underlying mechanism of action is not clear. In this study, we investigated the effect of CBD on the TME. We found that CBD reprogrammed TAMs from an immunosuppressive M2 profile into an antitumorigenic M1 profile and improved the therapeutic outcome of cancer immune therapies. Further experiments revealed that CBD induced metabolic reprogramming of macrophages via the phosphatidylinositol 3-kinase (PI3K)-protein kinase B (Akt) signaling. Our results highlight the role of CBD in modulating the immunosuppressive microenvironment during tumor progression.

## 2. Materials and methods

### 2.1. Reagent

CBD was purchased from ZZStandards (ZT-71, 836; Shanghai, China). Antibodies of Ki67 (Cat# 12202), p-PI3K (Cat# 4228), PI3K

(Cat# 4257), p-Akt (Cat# 4060), Akt (Cat# 4601), and p62 (Cat# 23214) were purchased from Cell Signaling Technology (Danvers, MA, USA). Antibodies of proliferating cell nuclear antigen (Cat# sc-25280), STAT6 (Cat# sc-374021), and Janus kinase (JAK)1 (Cat# sc-376996) were purchased from Santa Cruz Biotechnology (Dallas, TX, USA). Antibodies of p-JAK1 (Cat# ab138005) and pSTAT6 (Cat# ab263947) were purchased from Abcam (Cambridge, UK). Antibodies of inducible NO synthase (iNOS) (Cat# 4060) were purchased from ABclonal Technology (Wuhan, China). Antibodies of LC3B (Cat# NB100-2220) were purchased from Novus Biologicals (Beijing, China). Flow cytometry antibodies of CD206-PE (Cat# 141705), CD86-BV421 (Cat# 305425), CD8a-BV421 (Cat# 100737), CD4-PE-Cy7 (Cat# 100421), and granzyme B-AF647 (Cat# 515405) were purchased from BioLegend (San Diego, CA, USA). Flow cytometry antibodies of CD45-AF700 (Cat# 56-0451-82), perforin-APC (Cat# 17-9392-80), and perforin-PE (Cat# 12-9392-82) were purchased from Thermo Fisher Scientific Inc. (Waltham, MA, USA). Lipofectamine 3000 and Lipofectamine RNAi MAX were purchased from Thermo Fisher Scientific Inc.. Mouse IL-4 (Cat# 78047.1) was purchased from R&D Systems (Minneapolis, MN, USA). Recombinant human IL-4 (Cat# CX03) was purchased from Novoprotein Scientific Inc. (Beijing, China). The antibodies of anti-mouse PD-1 (Cat# BE0146) were purchased from Bio X Cell (Lebanon, NH, USA). Clodronate liposomes (Cat# 40337ES08) were purchased from Yeasen Biotechnology (Shanghai) Co., Ltd. (Shanghai, China). Matrigel (Cat# 356231) was purchased from Corning Inc. (Corning, NY, USA). Organoid growth medium (Cat# KCW-2) was purchased from Kingmed Pharm (Chongqing, China).

### 2.2. Mice and colon cancer xenograft model

C57BL/6 mice (female, 6–8 weeks old, 20–22 g) were purchased from GemPharmatech (Nanjing, China) and housed under optimal conditions of light, temperature, and humidity with free access to food and water. All animal experiments were conducted in strict accordance with the Guide for the Care and Use of Laboratory Animals and the relevant ethics regulations of Jiangsu Province and Nanjing University (Approval No.: IACUC-2204006). MC38 cells ( $1 \times 10^6$ ) were inoculated subcutaneously into the right flank of the mice. Tumor dimensions were measured by caliper every other day ( $V = \text{length} \times \text{width}^2/2$ ) and the mice were divided when the tumors grew to  $100 \text{ mm}^3$ . The MC38 tumor-bearing mice were treated with vehicle or different doses of CBD (intraperitoneally, daily) for a set number of days, and 5-fluorouracil (5-Fu, every other day) was intraperitoneally injected as a positive control. For the combination experiments, the MC38 tumor-bearing mice were treated with vehicle (intraperitoneally, every day), CBD (10 mg/kg, intraperitoneally, every day), anti-PD-1 (200  $\mu\text{g}/\text{mouse}$ , intraperitoneally, every three days), or a combination of CBD and anti-PD-1. Following a set number of days, the tumor-bearing mice were anesthetized, and tissues were harvested for further analysis and measurement. For macrophage depletion, the mice were injected i.t. with 150  $\mu\text{L}$  of clodronate liposomes or control liposome prior to tumor inoculation (day 0) and at days 3, 7, and 11 after subcutaneous tumor injection. Infiltrating macrophages ( $\text{F4}/80^+$ ) were assessed to ensure macrophage depletion.

### 2.3. Cell culture

Mouse colon cancer cell lines MC38 were maintained in our laboratory and were cultured at  $37^\circ\text{C}$  in a humidified incubator with 5%  $\text{CO}_2$  in Dulbecco's modified Eagle medium (DMEM) containing 10% fetal bovine serum (FBS) with 100 units/mL penicillin and 100  $\mu\text{g}/\text{mL}$  streptomycin. Bone marrow cells were flushed out from the femurs and tibias of female C57BL/6 mice. After

centrifugation for 5 min at 300 g, erythrocytes were eliminated, and the remaining cells were differentiated for 6 days in the mouse macrophage culture medium (DMEM supplemented with 10% FBS, 100 units/mL penicillin, 100 µg/mL streptomycin, and 10 ng/mL macrophage-colony stimulating factor), culture fluid was exchanged with culture medium every three days, and adherent macrophages were harvested. For alternative activation of macrophages, bone marrow-derived macrophages (BMDMs) were stimulated with 20 ng/mL recombinant IL-4 for 24 h.

#### 2.4. Patient-derived organoid culture and co-culture

The human CRC organoids were constructed and cultivated by Kingmed Pharm [26]. Briefly, patient tissue samples acquired by the surgical operation were minced into pieces as small as possible using sterile scissors. Then, the tissue pieces were mixed thoroughly with Matrigel at the approximate ratio of 1:4 (V/V) on ice. Next, the tissue-Matrigel suspensions were seeded quickly in the multi-well plate to form hemispherical droplets and transferred into incubator 37 °C for 15 min. Then, 1 mL of culture medium (Kingculture™ organoid growth medium, Kingmed Pharm) was added to each well; the medium was changed every two to four days. Generally, organoids are passaged in about seven to ten days. For organoid-macrophage co-culture experiments, 25–40 organoids and  $5 \times 10^4$  macrophages were mixed in Matrigel and added dropwise to a multi-well plate. After the Matrigel solidified, an appropriate amount of medium was added. Photomicrographs were taken on the 4th day to record the growth of the organoids.

#### 2.5. Single-cell dissociation from mouse for single-cell RNA/ATAC-seq

Solid tumors from the mice were digested using a tumor dissociation kit (Miltenyi Biotec, Bergisch Gladbach, Germany) to obtain single-cell suspensions. Single-cell suspensions with a concentration of 1000 cells/µL were loaded on the 10x Genomics chromium controller single-cell instrument following the 10x Genomics manufacturer's protocol. Reverse transcription reagents, barcoded gel beads, and partitioning oil were mixed with the cells to generate single-cell gel beads in emulsions for reverse transcription.

#### 2.6. Single-cell RNA sequencing (scRNA-seq) data pre-processing and quality control

The scRNA-seq data for each experiment were processed with Cell Ranger v4.0.0 pipeline (10x Genomics) based on the mouse reference genome GRCm38 (mm10). Digital gene expression matrices were analyzed in R (v4.0.4), using the Seurat (v4.0.0) package [27]. Cells were filtered by the number of UniqueMolecular Identifiers (UMIs) (<100,000 UMIs), the number of genes (<6500 genes), and percentage of mitochondrial genes (“percent.mt” lower than 10%) before downstream analysis. Normalization was performed using *SCTransform* function [28] with regression of percentage of mitochondrial genes. For integration, 3000 shared highly variable genes were identified using the *SelectIntegrationFeatures* function [29]. Integration anchors were identified based on these genes using the *FindIntegrationAnchors* function with an SCT normalization method. The data were then integrated using the *IntegrateData* function. Principal component analysis (PCA) and uniform manifold approximation and projection (UMAP) dimension reduction with the top 30 principal components were performed. A nearest-neighbor graph using the 30 dimensions of the PCA reduction was calculated using *FindNeighbors* function, followed by clustering using *FindClusters* function with a resolution of 0.8.

#### 2.7. Identification of differentially expressed genes (DEGs) among clusters and annotating cell clusters

Candidate marker genes for each cell cluster were identified by the *FindAllMarkers* function. For each cluster of cells, group-specific differentially expressed genes were identified using the Wilcoxon rank sum test as implemented in *FindAllMarkers* function (min.pct = 0.1, logfc\_threshold = 0.1, test.use = “wilcox”) with the Seurat R package, and genes with average expression difference >0.5 natural log with  $P < 0.05$  were selected as marker genes.

For each cell cluster identified as above, a cell type was assigned to it by using a combination of differentially expressed genes and known gene signatures. The *FeaturePlot* function showed that the cluster specific marker genes *Pecam1*, *Col1a1*, *Lyz2*, and *Cd3d* were significantly enriched in cancer cells, stromal cells, myeloid cells and lymphocytes, respectively.

#### 2.8. Single-cell ATAC sequencing (scATAC-seq) data pre-processing and quality control

The scATAC-seq data were pre-processed by Cell Ranger-ATAC (v2.0.0) using the count command line. For the subsequent scATAC-seq data processing and analysis, the ArchR (v1.0.1) package was used [30]. The *addArchRGenome* (“mm10”) function was used for genome annotation and an arrow file was created using the *createArrowFiles* function with its default parameters. The *filterDoublets* function was used to remove the potential doublets and an ArchR project was created using the *ArchRProject* function with its default parameters. The Harmony package was then used to remove the batch effect via the *addHarmony* function [31]. For dimensionality reduction, the *addIterativeLSI* function in ArchR was used with its default parameters. For single-cell embedding, the *reducedDims* object in Harmony was selected, and the *addUMAP* function with the parameter “perplexity = 30” was used for visualization.

#### 2.9. Marker genes identification and cluster annotation

To identify the marker gene, the gene scores were calculated when creating the ArchR project and stored in the arrow file. The *getMarkerFeatures* function was then used to identify the cluster-specific “expressed” genes, using the default parameters. To visualize the marker genes in embedding, the *addImputeWeights* function was used to run the MAGIC [32] to smooth gene scores across the nearby cells. For track plot, the *plotBrowserTrack* function was used with its default parameters except for “tileSize = 100”.

#### 2.10. Peak calling and TF binding motif analysis

Before peak calling, the *addGroupCoverages* function was used with its default parameters to generate pseudo-bulk replicates. Then, the *addReproduciblePeakSet* function was used with its default parameters except for “genomeSize =  $2.7 \times 10^9$ ” to call accessible chromatin peaks using MACS2 (v2.2.7.1) [33]. For cell type specific peak analysis, the *getMarkerFeatures* function with peak matrix was used initially to identify marker peaks. Next, the *getMarkers* function with the parameter “cutOff = false discovery rate (FDR) ≤ 0.01 & log<sub>2</sub>(fold change) (FC) ≥ 1” was used to obtain the differential peaks. For transcription factor (TF) motif enrichment analysis, the *addMotifAnnotations* function was used to add the motif annotation to the ArchR project, and the *peakAnnoEnrichment* function with the “cutOff = FDR ≤ 0.1 & Log<sub>2</sub>FC ≥ 0.5” parameter was used to compute TF motif enrichment in differential peaks. For motif footprint analysis, the *getPosition*

function was used to obtain the positions with relevant motifs. Then, the *getFootprints* function was used to compute the interest motif footprints, using the function's default parameters. Finally, the footprint patterns were plotted using the *plotFootprints* function with its default parameters.

### 2.11. Integrated analysis of scRNA-seq and scATAC-seq data

In order to integrate scATAC-seq data with matched scRNA-seq data, the *FindTransferAnchors* function from the Seurat package was used, and the data were aligned using the *addGeneIntegrationMatrix* function of ArchR in “unconstrained integration” mode. From the results, it was found that most of the predicted scores were >0.5. To improve the accuracy of the predictions in order to better integrate the two datasets, the “constrained integration” mode was again used to integrate the scATAC-seq and scRNA-seq data. Briefly, the scATAC-seq data were annotated with cell types based on the gene scores of scATAC-seq. Then, a restricted list was created such that gene expression similarity was calculated only in the same cell type for both scATAC-seq and scRNA-seq. For peak to gene linkage analysis, the *addPeak2GeneLinks* function was used to compute peak accessibility and gene expression with the parameters “corCutOff = 0.45, resolution = 1”.

### 2.12. Pseudo-time lineage trajectory

The cell lineage trajectory of cancer cells was inferred by using Monocle2 (version 2.18.0) R package [34]. Monocle sorts cells by learning an explicit principal graph from the single-cell genomics data with reversed graph embedding, thereby robustly and accurately resolving complicated biological processes [35]. The *differentialGeneTest* function was used to derive DEG from each cluster, and, after the cell trajectories were constructed, differentially expressed genes along the pseudo-time trajectory were detected. All pseudo-time-dependent genes were visualized using the *plot\_pseudotime\_heatmap* function taking a CellDataSet object. Lineage trajectory plot and smooth expression curves based on CellDataSet were generated using *plot\_cell\_trajectory* and *plot\_genes\_in\_pseudotime*, respectively [36].

### 2.13. Enrichment analysis

Gene set enrichment analysis (GSEA) [37] was applied using 50 hallmark gene sets (h.all.v7.4.symbols.gmt) to identify significantly enriched functional pathways via the GSEA software (v4.1.0), with screening criteria of nominal *P*-value <0.05 and FDR *q*-value <0.25. The functional phenotypes of each macrophage subset were defined using gene set variation analysis (GSVA) with the GSVA package [38].

### 2.14. Cell-cell interaction analysis

Cell-cell interactions among the cell types was inferred through CellChat, a tool that can quantitatively infer and analyze intercellular communication networks from scRNA-seq data, delineating the specific signaling roles played by each cell type [39]. The *computeCommunProbPathway* function was used to compute the communication probability at the signaling pathway level by summarizing all related ligands/receptors with default parameters. The contribution of each ligand-receptor pair to the overall signaling pathways was computed and visualized using the *netAnalysis* contribution function.

### 2.15. Quantitative real-time polymerase chain reaction (qRT-PCR) analysis

Cells were washed three times with cold phosphate-buffered saline (PBS), and total RNA was extracted from the cells using the TRIzol reagent (Invitrogen, Waltham, MA, USA) according to the manufacturer's instructions. Single-stranded complementary DNA was synthesized from 1 µg of total RNA by reverse transcription. Real-time PCR was performed with SYBR Green Realtime PCR Master Mix (Vazyme Biotech Co., Ltd., Nanjing, China) on a CFX 100 (Bio-Rad, Hercules, CA, USA) cycler. The PCR cycling conditions were 95 °C for 3 min and 35 cycles at 95 °C for 30 s, 60 °C for 40 s, and 72 °C for 1 min. The expression of *β-actin* was used to normalize the data.

### 2.16. Western blot

Cells were washed three times with cold PBS and lysed with Western blot and immunoprecipitation lysis containing protease and phosphatase inhibitor cocktails (MCE, Shanghai, China). Protein concentration was determined using a bicinchoninic acid protein quantitation kit. Proteins extracted in lysis buffer were separated by 10%–12% sodium dodecyl sulfate-polyacrylamide gel electrophoresis and transferred onto polyvinylidene difluoride membranes. The membranes were blocked with 5% bovine serum albumin for 1 h at room temperature and probed with the indicated antibodies overnight at 4 °C. Then, the membranes were incubated with a horseradish peroxidase-coupled secondary antibody. Detection was performed using a LumiGLO chemiluminescent substrate system.

### 2.17. Flow cytometry

Single-cell suspensions were incubated with surface marker antibodies for 30 min on ice, and for intracellular cytokine staining, the cells were fixed and permeabilized using intracellular fixation and permeabilization buffer as per the manufacturer's instructions (eBioscience, Waltham, MA USA). The cells were then stained with intracellular antibodies for another 30 min on ice and analyzed using flow cytometry. In the case of intracellular cytokine staining, a cell stimulation cocktail (plus protein transport inhibitors) was added for 4 h before staining. Fluorochrome-conjugated antibodies were purchased from BioLegend, eBioscience, or BD Biosciences (San Diego, CA, USA). Data were acquired using the Attune NxT (Life Technologies, Waltham, MA USA) flow cytometer and analyzed with the FlowJo (BD Biosciences) software.

### 2.18. Macrophage apoptosis and proliferation analysis by flow cytometry

Annexin V staining kit (Sigma, Louis, MO, USA) was used to assess apoptosis in BMDMs. Cells were washed in 1 × binding buffer and stained with fluorescein isothiocyanate isomer I-conjugated annexin V and propidium iodide (PI) antibodies for 15 min and immediately assessed by flow cytometry.

### 2.19. Extracellular flux assays

The oxygen consumption rate (OCR) and extracellular acidification rate (ECAR) were measured using the Seahorse XF cell mito stress test kit (Agilent, North Billerica, MA, USA) or XF extracellular flux analyzer (Seahorse Bioscience, North Billerica, MA, USA). Briefly, BMDMs were plated onto Seahorse XF-96 cell culture microplates (5 × 10<sup>4</sup>/well) overnight, then cells were treated with or without CBD (10 µM) and polarized into M2 macrophages with

IL-4 (20 ng/mL) for 24 h. Cells were washed, and the medium was changed to XF assay medium (unbuffered DMEM pH 7.4 supplemented with 10 mM glucose, 1 mM sodium pyruvate, and 2 mM GlutaMAX for OCR, and 1 mM sodium pyruvate and 2 mM GlutaMAX for ECAR), then cells were incubated in a non-CO<sub>2</sub> incubator for 1 h following the manufacturer's instructions. Real-time measurement of OCR and ECAR were performed using the Seahorse 96-well extracellular flux analyzer (Agilent) according to the manufacturer's instructions and as previously described. To assess mitochondrial respiration, three to four consecutive measurements were obtained under basal conditions and following the sequential addition of 1 μM oligomycin, to inhibit mitochondrial adenosine triphosphate (ATP) synthase; 1.5 μM fluoro-carbonyl cyanide phenylhydrazone, a protonophore that uncouples ATP synthesis from oxygen consumption by the electron transport chain; and 100 nM rotenone plus 1 μM antimycin A, which inhibit the electron transport chain. To assess glycolysis rates, 100 nM rotenone plus 1 μM antimycin A were injected to inhibit mitochondrial oxygen consumption, and 50 mM 2-deoxy-D-glucose was injected to inhibit glycolysis through competitive binding of glucose hexokinase.

#### 2.20. ATP measurement

ATP was assayed using the ATP detection assay kit (Beyotime, Shanghai, China) according to the manufacturer's instructions. Briefly, BMDMs were stimulated with IL-4 and treated with or without CBD for 24 h. Cells were harvested and lysed using ATP detection lysate. The fluorescence intensity was detected by a luminometer.

#### 2.21. In vitro macrophage and tumor cell co-culture assay

A 24-well glass-bottomed plate was coated with fibronectin (1:100, V/V). Macrophages were seeded ( $1.5 \times 10^5$ /well) to the plate and treated with medium or IL-4 (20 ng/mL) for 24 h with or without CBD treatment. The next day, the medium was discarded, and the cells were washed with PBS then labeled with 5(6)-carboxyfluorescein diacetate succinimidyl ester. MC38 tumor cells expressing mCherry fluorescent protein were seeded ( $5 \times 10^4$ /well) to the plate. The culture medium was changed from a macrophage culture medium to a cancer cell medium. After 48 h, live cell imaging was performed.

#### 2.22. Immunohistochemistry and immunofluorescence staining

Paraffin-embedded slides of tumor sample were dewaxed in xylene and rehydrated through 100%, 75%, and 50% ethanol, and then the antigen was repaired using sodium citrate. For immunohistochemical staining, slides were additionally treated with 3% hydrogen peroxide to eliminate endogenous peroxidase activity. After blocking with 5% goat serum, the slices were incubated with antibodies overnight at 4 °C. The anti-mouse/rabbit horseradish peroxidase-labeled polymer (100 μL) was added, and samples were incubated at 37 °C for 30 min, followed by 100 μL of 3,3'-N-diaminobenzidine tetrahydrochloride working solution and incubation at room temperature for 5 min. After 1 min of staining with hematoxylin, samples were washed in 50%, 75%, and 100% ethanol and xylene for 5 min, and neutral gum was used to seal the film. The film was observed and photographed under a microscope.

For immunofluorescence staining, slides were washed with PBS and stained with fluorophore-conjugated secondary antibodies (1:500, V/V) at room temperature for 90 min and counter-stained with 4'-6-diamidino-2-phenylindole for 2 min. After washing five times, the cells were observed with a confocal laser scanning

microscope (LSM880, Zeiss, Oberkochen, Germany).

#### 2.23. Statistics

Statistical analysis was performed using GraphPad Prism 8.0. All results are expressed as the mean ± standard error of mean. Student's *t*-test was used to evaluate the significant difference between the two groups. One-way analysis of variance followed by Dunnett's post hoc test were used to evaluate the differences when there were more than two groups. Statistical significance was set at \**P* < 0.05; \*\**P* < 0.01; and \*\*\**P* < 0.001 (ns: no significance).

#### 2.24. Data availability

The raw data for the single-cell RNA-seq samples are available in the Gene Expression Omnibus database (Accession No.: GSE220635).

### 3. Results

#### 3.1. CBD inhibits the growth of transplanted colon cancer in mice

To explore the effect of CBD on the growth of MC38 xenografts in mice, we treated mice with different doses of CBD on the seventh day after transplantation, and 5-Fu was used as a positive control. The results showed that both tumor volume and tumor weight were significantly decreased by CBD treatment in a dose-dependent manner (Figs. 1B–D), while there was no difference in the body weight between CBD and vehicle mice (Fig. S1A). Furthermore, histological evaluation of the tumor revealed that CBD treatment resulted in sparse arrangement and fragmentation of the tumor cells, indicating apoptosis in varying degrees (Fig. S1B). Moreover, we detected cell apoptosis by terminal deoxynucleotidyl transferase dUTP nick-end labeling (TUNEL) staining. The results showed that more TUNEL-positive cells were detected in the CBD treatment group than in the vehicle group (Figs. 1E and F). Notably, the expression of Ki67 in tumor tissues was noticeably reduced in the CBD treatment group (Figs. 1G and H). In addition, CBD also increased the expression of *Ifnγ*, *Granzyme B* (*Gzmb*), *Perforin*, and *Fas ligand* (*FasL*) in tumors (Fig. S1C). Taken together, these results suggest that CBD inhibits the growth of colon cancer in mice.

#### 3.2. Single-cell analyses reveal CBD remodels TME in MC38 transplanted tumor

Previous studies have reported that CBD inhibits tumor cell proliferation [21,22], but the effect of CBD on the TME remains unclear. Therefore, we performed scRNA-seq and scATAC-seq to explore the impact of CBD on MC38 colon cancer. We collected the single cells from murine MC38 xenograft tumors in vehicle and CBD treatment groups and performed matched scRNA-seq and scATAC-seq analyses (10x Genomics) (Fig. 2A). After quality control and filtering, a total of 20,363 cells met the preprocessing threshold and were used for downstream analysis (Figs. S2A and B). We demonstrated the overall high quality of scATAC-seq data based on the enrichment analysis of accessible DNA sequences relative to the transcriptional start site and the size distribution of unique fragments (Figs. S2C and D). The cell population in TME was divided into five major cell types by their gene expression signatures, including cancer cell, fibroblast cell, myeloid cell, lymphoid cell, and endothelial cell (Figs. 2B and C). Unsupervised clustering with UMAP annotated 15 sub-cell clusters by known or putative markers (Figs. 2B–D). We compared the changes in the number of various

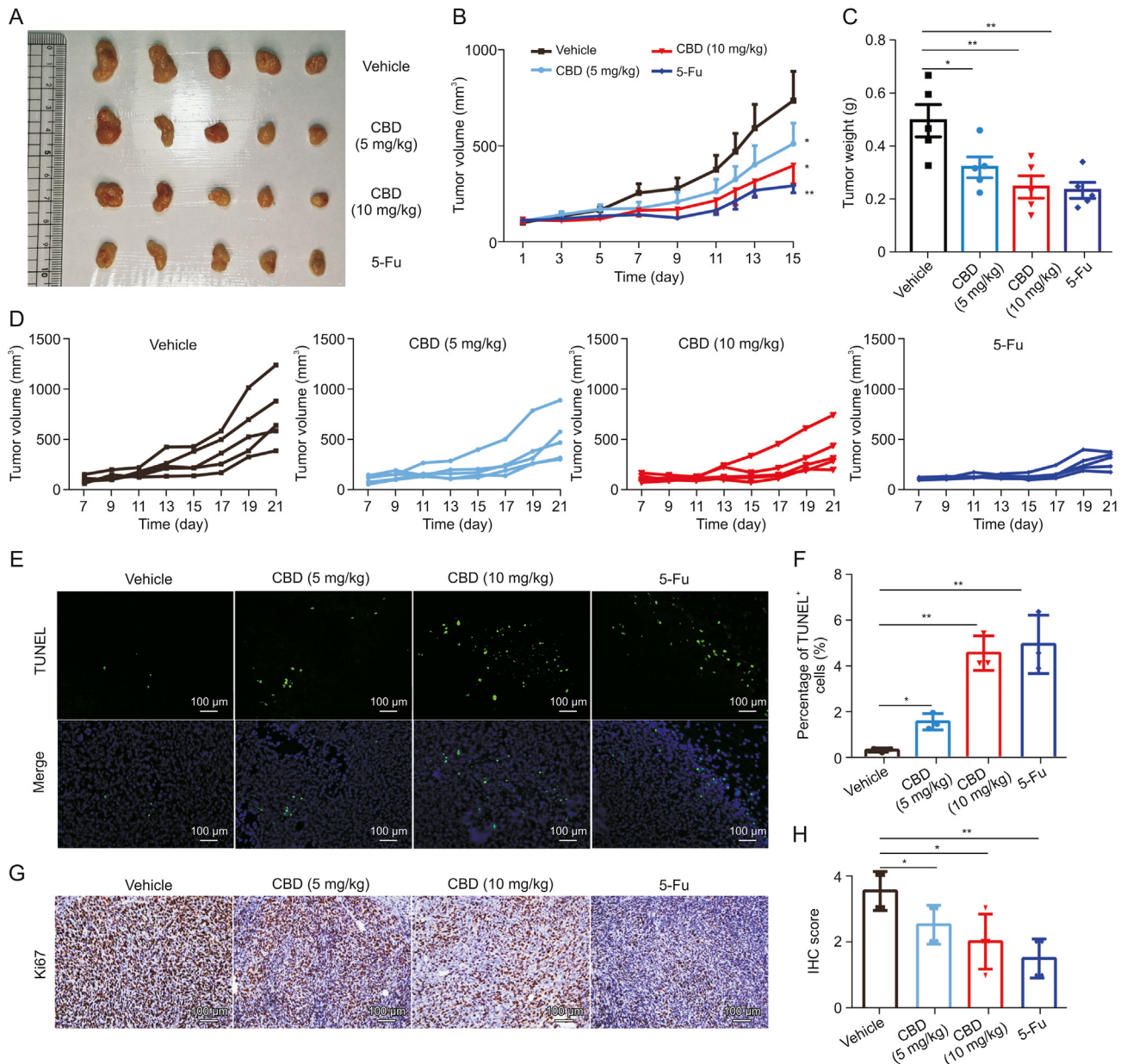


**Fig. 1.** Cannabidiol (CBD) inhibits the growth of transplanted colon cancer in mice. MC38 cancer cells ( $1 \times 10^6$ ) were inoculated subcutaneously into each mouse ( $n = 5$ ). When the tumor grew to 100 mm<sup>3</sup>, the mice were randomly divided into a vehicle group (i.p., once a day), a 5-fluorouracil (5-Fu) group (25 mg/kg, i.p., once every other day), and a CBD different dose group (5 mg/kg and 10 mg/kg, i.p., once per day). (A) Representative images of the tumor. (B) Tumor growth curve. (C) Tumor weight. (D) Tumor volumes of individual mice. (E, F) Terminal deoxynucleotidyl transferase dUTP nick-end labeling (TUNEL) assay for apoptotic cells in tumor tissue. (G, H) Immunohistochemistry (IHC) for detecting Ki67 in the tumor tissue. Data are represented as mean  $\pm$  standard error of mean. \* $P < 0.05$  and \*\* $P < 0.01$ .

cell types in the vehicle and CBD treatment groups. In addition to a decrease in the number of tumor cells (from 22.85% to 16.8%), the number of lymphocytes (from 1.84% to 3.14%) and myeloid cells (from 10.85% to 11.72%) increased in the CBD-treated group (Fig. 2E). The proportions of 15 cell subpopulations and the number of differential genes from the vehicle and CBD groups, respectively, showed that the number of cancer cell subpopulations after CBD treatment decreased significantly, and the total number of differential genes increased significantly (Fig. S3A). We analyzed cell-cell interactions and found that CBD significantly enhanced individual cell-cell interactions, including tumor cells and CD8<sup>+</sup> T cells, tumor cells and nature killer (NK) cells, tumor cells and macrophages, and macrophages and CD8<sup>+</sup> T cells (Fig. 2F).

In particular, the interaction between cancer cells and

macrophages in the CBD group was significantly enhanced. To address the question of whether cellular communication was enhanced in the cells of the vehicle and CBD groups, we calculated the integrated cellular communication network by counting the number of links between the vehicle and CBD groups and summarizing the communication probabilities. We found that the number and intensity of interactions between the CBD group were significantly higher than that of the vehicle group, and the interaction between cancer cells and macrophages was significantly higher. The number or total interaction strength were also significantly enhanced (Figs. S3B and C). These data show differences in the landscape of vehicle and CBD in cancer cells and macrophages, suggesting the potential effects of CBD on macrophages. Taken together, our results reveal that CBD treatment significantly alters

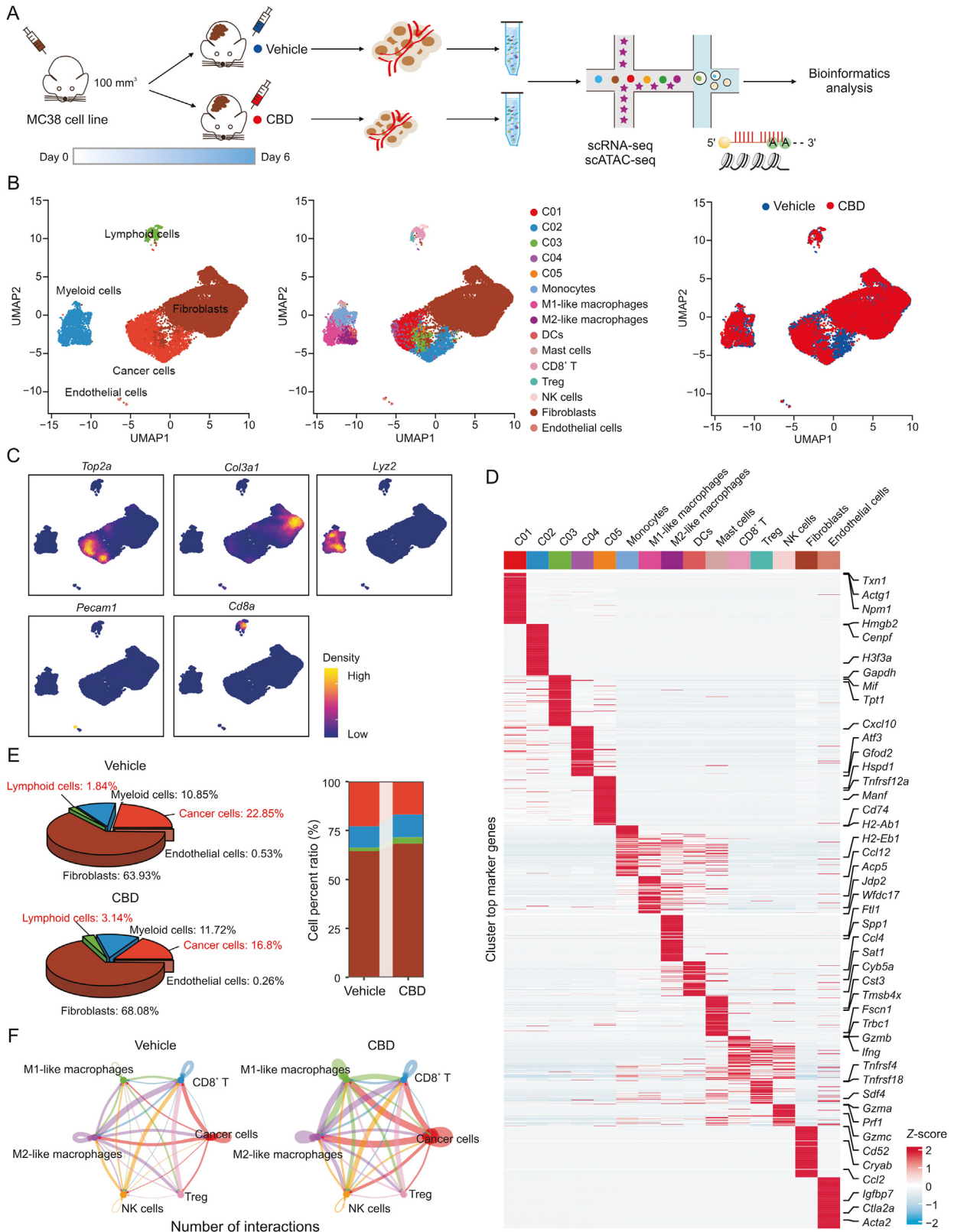


**Fig. 2.** Single-cell RNA sequencing (scRNA-seq) analysis of cannabidiol (CBD) inhibiting the growth of MC38 transplanted tumor. (A) Schematic diagram of scRNA-seq and single-cell ATAC sequencing (scATAC-seq). (B) The uniform manifold approximation and projection (UMAP) visualization shows unsupervised scRNA-seq clustering, revealing 5 major clusters (left) and 15 minor clusters (middle) in two groups (right). (C) Expression of example marker genes. (D) Heatmap of row-wise Z-score-normalized mean expression of selected marker genes. (E) 3D pie chart of the major cluster proportion in vehicle and CBD. (F) The overall networks of cell-cell communication within myeloid sub-populations between vehicle and CBD. DCs: dendritic cells; NK: nature killer; Treg: regulatory T cells.



the TME as well as the intercellular interactions within the microenvironment.

### 3.3. CBD treatment alters macrophage signature in the TME

As mentioned above, CBD treatment profoundly affected the proportion of myeloid cells in the tumor and enhanced the interaction between cancer cells and macrophages (Figs. 2E and F). Therefore, we further divided myeloid cells into five sub-clusters based on gene expression. To our surprise, the number of infiltrating M1-like macrophages in tumors was significantly increased after CBD treatment, whereas M2-like macrophages were significantly decreased (Figs. 3A and B). Therefore, we compared the differentially expressed genes of M1- and M2-like macrophages in the two groups of vehicle and CBD groups and found that pro-inflammatory macrophage activation-related genes such as *Nos2*, *Cd80*, *Cd86*, and *I12b* were significantly up-regulated, which means that the macrophages enhanced anti-tumor ability. Consistent with this, in M2 macrophages, we observed significant downregulation of *Cd9*, *Cebpb*, and *Spp1* genes, which have been shown to induce the M2 phenotype in macrophages. In particular, we found that CBD significantly induced the expression of glycolysis-related genes in macrophages, including *Aldoa*, *Ldha*, and so on. (Fig. 3C). These results indicate that CBD treatment significantly affected the function of macrophages in tumors.

Next, we explored the differentiation relationship between monocytes and macrophage subpopulations through pseudo-chronological analysis. We found that macrophages differentiated from monocytes and that M2-like macrophages tended to polarize toward M1-like macrophages as the pseudo-chronology progressed (Figs. 3D–F). The heatmap analysis shows the distribution of monocytes and macrophage subtypes during the transition (divided into three phases) along with the pseudo-time. We found that some genes related to macrophage polarization were also involved in this process (Fig. S4A). Moreover, through the analysis of cell communication, we found that compared with the vehicle group, the number or intensity of interactions between cancer cells and M1- and M2-like macrophages was significantly enhanced in the CBD treatment group (Fig. 3G).

To explore the effect of CBD treatment on macrophages and the specific anti-tumor mechanism, we performed gene enrichment analysis on M1- and M2-like macrophages, respectively (Figs. 3H and I). Among M1-like macrophages, glycolysis, inflammatory response, and reactive oxygen species (ROS) pathways were significantly enriched after CBD treatment (Fig. 3H). Among M2-like macrophages, signaling pathways such as PI3K-Akt, oxidative phosphorylation, fatty acid metabolism, and cholesterol homeostasis were down-regulated (Fig. 3I). These results indicate that CBD significantly altered the metabolic and antitumor functions of macrophages. To account for the underlying biological complexity in which genes may belong to multiple annotation categories, we characterized the connections between genes and pathways as a network by cnet plot, showing the possible downstream of pathways enriched by M1- and M2-like macrophages target genes, and we found that M1-like macrophages up-regulated the target genes related to glycolysis, inflammatory response, and the active oxygen pathway, and correspondingly, M2-like macrophages down-regulated the downstream target genes related to PI3K-Akt-mechanistic target of rapamycin (mTOR) and the cholesterol homeostasis pathway (Figs. 3J and K). These results suggest that CBD induces an anti-tumor effect by changing the metabolism of macrophages.

Next, we ranked critical signaling pathways based on the difference in overall information flow in the network inferred between the vehicle and CBD. We found that CBD treatment significantly enhanced intercellular communication. As one of the T

cell co-stimulatory signals, antigen-presenting cells express CD86 and bind to the T cell surface receptor CD28 to initiate T cell activation. Our results showed that CBD significantly enhanced CD86 signaling (Fig. S3D). We further mapped ligand-receptor pairs in specific cell subpopulations. We observed that the interaction between H2-k1-Cd-8a and H2-k1-Cd8b1 between tumor cells and T cells was enhanced, indicating that CBD treatment increases the recognition and killing of tumor cells by T cells in tumors. In particular, the interaction between Mif-(CD74-CD44) and App-CD74 was significantly enhanced between tumor cells and macrophages, suggesting enhanced antigen presentation and phagocytosis by macrophages after CBD treatment (Fig. S3E). Collectively, our results suggest that CBD inhibits colorectal cancer progression by modulating macrophage function.

### 3.4. Identification of specific regulators of M1- and M2-like macrophages

To identify potential transcriptional regulators of M1- and M2-like macrophages, we employed pySCENIC to decipher the gene regulatory network modules specific to each sample based on co-expression and motif enrichment. We analyzed representative TF regulons across M1- and M2-like macrophages. The scatter plot and heatmap showing the top regulons of M1- and M2-like macrophages ordered by regulon-specific score and top regulons with high activity are highlighted (Figs. 4A and B). Then, we analyzed the signatures associated with macrophages by GSVA, the heatmap showing different expression patterns of the indicated signature genes among myeloid subtypes. The results showed that M1-like macrophages have a pro-inflammatory effect in contrast to M2-like macrophages, which have the function of anti-inflammation.

Moreover, different macrophage subtypes showed apparent heterogeneity in M1- and M2-polarization (Fig. 4C). Next, we visualized the top 10 TF regulons and their targeted genes between vehicle and CBD, as shown in Figs. 4A and B by gene regulatory networks (Fig. 4D). We examined the effect of CBD on these transcription factors in macrophages in vitro and found that STAT3 and NF-κB signaling were significantly enhanced after CBD treatment (data not shown). It has been reported that STAT3 NF-κB signaling directly and indirectly regulate various metabolism-related processes, including glycolysis [40,41]. The dot plot showed that inflammation-related genes are highly expressed in M1-like macrophages, which echoes the pro-inflammatory function of M1-type macrophages itself, and also confirms the results of Fig. 4C, indicating that CBD promotes the inflammatory response of M1-like macrophages to better help the body clear tumors in the anti-tumor process (Fig. 4E). As mentioned above, under the action of CBD, the glycolytic pathway was significantly enriched in M1-like macrophages (Fig. 3H).

Next, we wanted to see if the glycolytic pathway was also altered in M2-like macrophages. A raincloud plot was generated, showing selected glycolysis-related gene differences in M2-like macrophages from the vehicle and CBD groups. The results showed that CBD up-regulated the glycolysis of M2 macrophages, implying that CBD might transform M2-like macrophages into M1-like macrophage characteristics by promoting glycolysis (Fig. 4F).

### 3.5. Single-cell chromatin landscape of major organs in vehicle and CBD treatment groups

To deconstruct the gene regulation principles of M1-like macrophages in CBD, we examined the single-cell chromatin accessibility landscape of vehicle and CBD by scATAC-seq. In total, we generated open chromatin profiles from 11,967 individual cells after quality control (Figs. S2C and D). To explore the gene regulatory

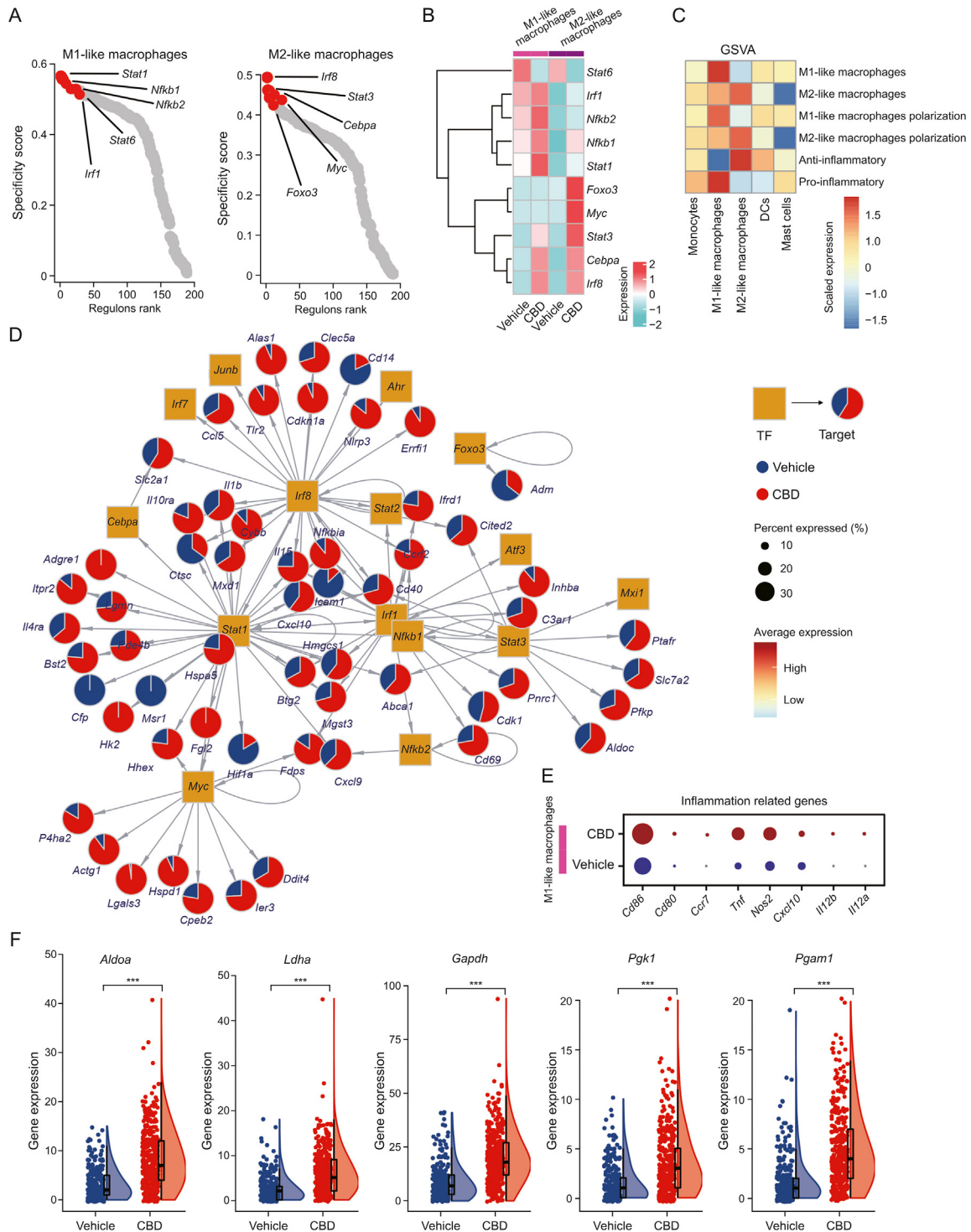


**Fig. 4.** Identified specific regulators of the maintenance of macrophage subtypes identity. (A) Dot plot showing the transcription factor (TF) regulons that regulate macrophage subtypes predicted by pySCENIC. The top five TFs are highlighted. (B) Heatmap showing the enrichment of the TF in specific macrophage subtypes between vehicle and cannabidiol (CBD). (C) Heatmaps showing different expression patterns of the indicated signature genes among myeloid subtypes calculated by gene set variation analysis (GSVA). (D) Gene regulatory networks (GRNs) by the top 10 TF regulons and their targeted genes. TF regulons are highlighted by yellow rectangles, and target genes are shown by circles. Pie charts of nodes indicate the relative gene expression level between the two groups. (E) Dot plot showing the inflammation-related genes in M1-like macrophages between the two groups. (F) Raincloud plots showing the selected gene expression difference for M2-like macrophages from vehicle and CBD groups. Data are represented as mean ± standard error of mean. \*\*\**P* < 0.001. DCs: dendritic cells.

programs in CBD, we integrated the gene accessibility and gene expression data using ArchR [30]. We observed that most of the ATAC peaks (*cis*-regulatory elements (CREs)) demonstrated differential accessibility among cell clusters (Figs. S4D and F), confirming

distinctive chromatin landscapes in different cell types. We identified five distinct cell clusters in the integrated cell map according to cluster-specific *cis*-elements and visualized the single-cell profiles with UMAP (Fig. S4B). The UMAP plot shows the distribution of

marker genes in cell types (Fig. S4C). Next, we extracted myeloid cells and identified five distinct cell clusters in the integrated cell map by integrating with scRNA-seq (Figs. 5A and B). For example, myeloid cells demonstrated accessibility at *cis*-elements neighboring cell type genes, such as monocytes (*Cd14*), M1-like macrophages (*Cd86*), M2-like macrophages (*Cd163*), dendritic cells (*Clec9a*), and mast cells (*Kit*) (Fig. 5C). We detected 196,211 *cis*-elements across all cell clusters, ranging from 12,285 to 94,861 peaks in each cluster (Fig. 5D). Next, we correlated the motif activity with the expression level of the corresponding TFs to systematically deduce either positive or negative TFs controlling colon development based on whether TF expression was positively or negatively correlated with their motif enrichment. The top 15 representative activators are highlighted in Fig. 5E, including cell identities such as *Stat1*, *Stat3*, *Irf3*, and *Irf5* for M1-like macrophages (Fig. 5F), which play crucial roles in maintaining M1-macrophage characteristics and cell fate specification. In addition, the dot plot shows that the genes related to M1-like macrophages were significantly enriched in the CBD group (Fig. 5G). Generally, the expression of these factors was closely correlated with the accessibility of open chromatin regions and their binding motif enrichment (Fig. 5H).

Furthermore, we sought to demonstrate the power of scATAC-seq data for reconstructing cellular developmental trajectories in CBD, which analysis would allow identifying key regulators for macrophage development at a cell-type level. CREs and TFs make up the regulatory logic determining the cell state transition. To study CREs for cell type-specific transcriptional programs, we identified a total of 56,287 CRE-gene pairs (peak-to-gene links) in the ATAC-RNA integration cell clusters (Fig. S4E). We focused on the developmental trajectory of M1-like macrophages, and the CRE accessibility in the promoter and distal enhancers of *Stat1* gradually increased from the early to the intermediate and then to the effector states (Fig. 5I). To identify positive TF regulators driving M1-like macrophage differentiation, we analyzed the dynamics of gene scores, expression, and CRE accessibility, as well as TF motif enrichment, across the differentiation trajectory (Fig. S4G). Then, we integrated motif accessibility with similarly dynamic gene scores or gene expression patterns across the trajectory. We found that *Stat1*, *Stat3*, *Stat6*, *Irf4*, and *Irf5*, the factors critical for M1-like macrophage lineage specification, showed sequential activities (Fig. 5J). Collectively, our scATAC-seq data provide a rich resource for the unbiased discovery of regulatory DNA elements associated with cell types, especially macrophages.

### 3.6. CBD enhances the killing function of immune cells

To address the potential role of macrophages in the anti-tumor effect of CBD, we depleted macrophages by intravenous injection of clodronate liposome (Figs. S5A and E). We observed that CBD treatment no longer significantly inhibited tumor growth after macrophage depletion (Figs. S5B–D). These results indicate that the anti-tumor effect of CBD is at least partly macrophage-dependent.

Next, we investigated the specific mechanism of CBD that leads to the enhancement of immune cell function that plays an anti-tumor role. To explore this, we analyzed lymphocytes and further divided them into three sub-clusters based on gene expression (Figs. S6A and D). The results show that CBD decreased the ratio of regulatory T cells (Tregs) and promoted the infiltration of CD8<sup>+</sup> T cells and NK cells (Fig. S6B). Moreover, through the analysis of cell communication, it was found that compared with the vehicle group, the number or intensity of interactions between cancer cells with CD8<sup>+</sup> T cells and NK cells was significantly enhanced (Fig. S6C). Next, we analyzed the global signaling patterns of cell communication between the vehicle and CBD treatment groups by Cellchat. Overall, CBD treatment reduced *Spp1* signaling in M2 macrophages,

which has been shown to prevent lymphocyte infiltration and may contribute to tumor immunotherapy resistance [42]. In addition, CBD treatment also significantly enhanced complements signaling in macrophages, suggesting that CBD promotes the anti-tumor function of macrophages (Fig. S6E). As TAMs have been shown to suppress T- and B-cell function through multiple actions, the effect of CBD on macrophages prompted us to be further curious about the impact of CBD on the suppressive tumor microenvironment. CBD treatment significantly promoted the expression of multiple associated proteases with lymphocyte homing and activation, such as  $\alpha$ -selectin (*Cd62l*, encoded by *Sell*) and Cd69 (encoded by *Cd69*) (Fig. S6F). Based on the above results, we infer that CBD enhances the recognition and killing function of immune cells by activating CD8<sup>+</sup> T cells and NK cells.

### 3.7. CBD suppresses alternative activation of macrophage in vitro

To validate the results of the scRNA-Seq analysis, we detected the number of macrophages in the tumor tissues by immunofluorescence. From this, we observed that CBD treatment decreased the number of CD206<sup>+</sup> macrophages in tumors while appropriately increasing the number of iNOS<sup>+</sup> macrophages (Fig. 6A). To explore the effect of CBD on macrophages, we first investigated whether CBD treatment regulates macrophage survival in vitro. The results showed that CBD treatment did not affect the proliferation and apoptosis of macrophages (Figs. S7A and B). In addition, CBD treatment did not induce autophagy in macrophages (Fig. S7C). Cytokines abundant in the tumor microenvironment, such as IL-4 and IL-13, have been shown to induce the differentiation alternatively activated macrophage that displays the expression of proteins associated with anti-inflammation, including arginase-1 (*Arg1*), resistin-like molecule- $\alpha$  (*Retnla*), or chitinase 3-like1 (*Chi3l1*) [43]. Next, we examined the role of CBD in macrophage polarization after IL-4 stimulation in vitro. We found that CBD treatment significantly reduced the expression of CD206, a specific marker of the M2 macrophage, but increased the expression of CD86, a marker gene of the M1 macrophage, in a dosed manner (Figs. 6B and S7D). This result was confirmed by detecting the expression of anti-inflammatory signature genes such as *Arg1*, *Cd206*, *Chi3l1*, and *Retnla* by qRT - PCR (Figs. 6C and S7E). We also monitored the expression of these genes in a RAW264.7 cell line of IL-4 stimulation over a time course and found that the anti-inflammatory-associated gene expression in CBD treatment cells was reduced at the early phase (data not shown). Notably, CBD treatment increased the expression of *Il12b* and *Nos2*, the marker of M1 macrophages' tumoricidal activity (Fig. 6D). In addition, immunofluorescence examination of the polarization of macrophages after CBD treatment showed that CBD treatment decreased the level of CD206 and increased the level of iNOS in BMDMs (Figs. 6E and F). Moreover, we co-cultured fluorescently labeled IL-4-polarized macrophages with mCherry-expressing tumor cells and found that CBD treatment significantly reduced the number of tumor cells (Figs. 6G, S7F, and S7G). Collectively, our data indicate that CBD inhibits the activation of alternatively polarized macrophages and promotes macrophages' anti-tumor effects.

In order to further explore whether the pharmacological effects of CBD in mice also have a potential for clinical therapeutics, we examined the effect of CBD on the M2 polarization of human macrophages. Consistent with the results of mice, CBD inhibited the M2 polarization of human macrophages (Fig. S7H). Meanwhile, we also determined the pharmacological effects of CBD through the organoid-macrophage co-culture model (Fig. S7I). We co-cultured IL-4-primed macrophages with human colorectal cancer organoids and found that IL-4-primed macrophages significantly promoted organoid growth, whereas CBD-treated macrophages were sufficient to

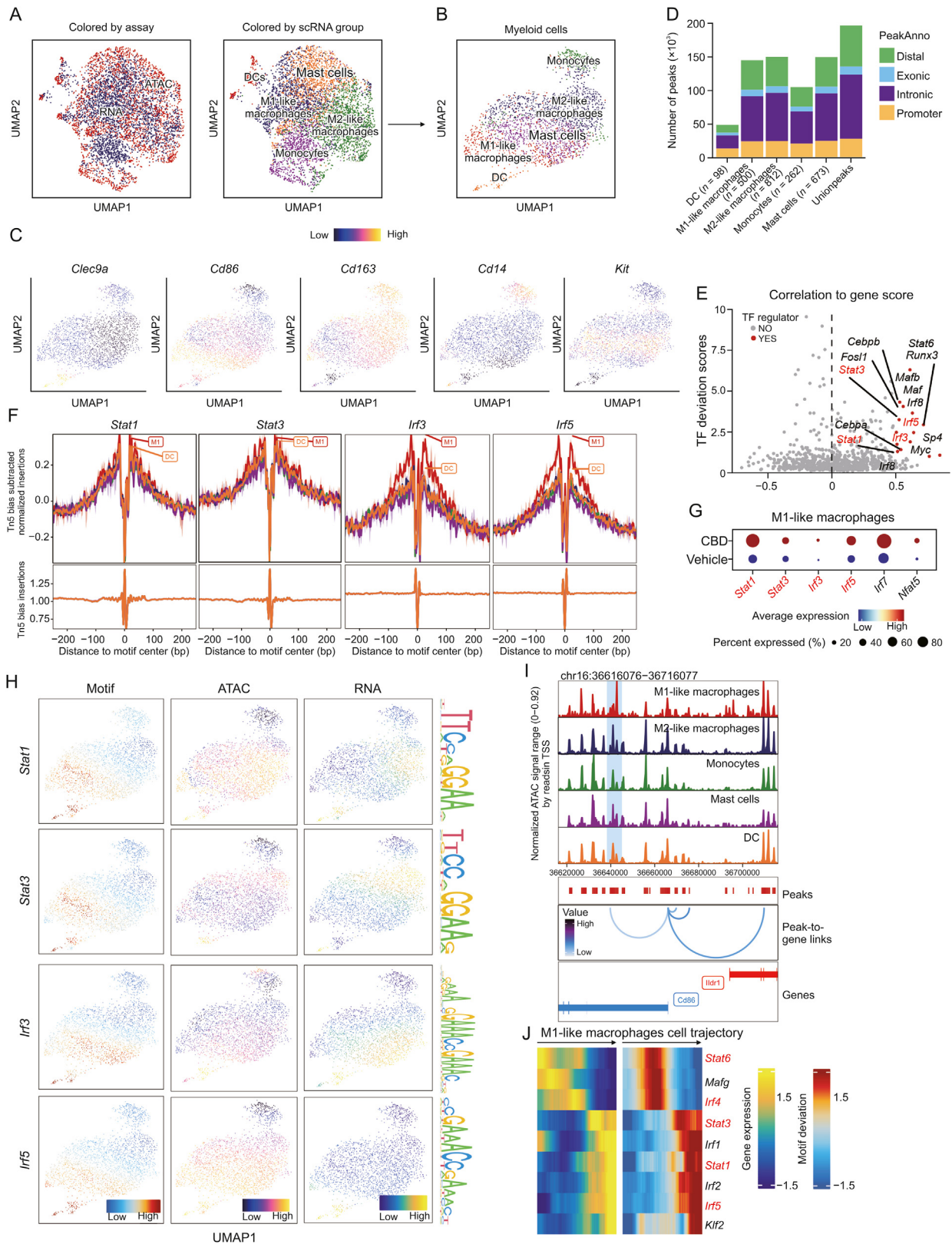


**Fig. 5.** Integrative analysis of myeloid cells of single-cell RNA sequencing (scRNA-seq) and single-cell ATAC sequencing (scATAC-seq) data in the vehicle and cannabidiol (CBD) treatment group. (A, B) Uniform manifold approximation and projection (UMAP) plot showing the joint clustering of scRNA-seq (blue) and scATAC-seq (red) data in colon. Cells in the right UMAP are colored based on cell types annotated by scRNA-seq data. (C) Marker genes expression based on scATAC-seq data. (D) Bar plot showing the number of reproducible peaks identified from each cluster. The peaks are classified into four categories: distal, exonic, intronic, and promoter. (E) Dot plot showing the identification of positive transcription factor (TF) regulators through correlation of chromVAR TF deviation scores and gene expression in cell groups (Pearson correlation  $r > 0.5$ , adjusted  $P$ -value  $< 0.01$ , and deviation difference in the top 25th percentile). (F) TF footprint for the *Stat1*, *Stat3*, *Irf3*, and *Irf5* motif with the subtraction using the Tn5 bias normalization method. (G) Dot plot showing the M1-like macrophage-related genes between the two groups. (H) Profile of the *Stat1*, *Stat3*, *Irf3*, and *Irf5* TF motif activity, gene chromatin accessibility, and gene

inhibit organoid growth (Figs. 6H and S7J). These results show that the data we obtained in mice could be applied to humans.

### 3.8. CBD alters the metabolic processes in macrophages by inhibiting PI3K/Akt signaling

M2 polarization integrally involves the activation of STAT6, which potentiates M2-specific polarization by the transcriptional up-regulation of *Arg1*, *Cd206*, and *Fizz1* [44]. As an immunosuppressive inflammatory factor, IL-4 interacts with its receptor IL-4R to activate the downstream JAK-STAT6 signal, and the activated STAT6 enters the nucleus to induce the expression of anti-inflammatory-related genes. To determine the effect of CBD on STAT6 activity, we evaluated the activation status of STAT6 under M2-polarization conditions. The results showed that CBD did not alter the phosphorylation of STAT6 either in a time or dose course (Figs. S8A and B).

Distinct metabolic programs are necessary to control macrophage polarization by supporting the associated energy demands, leading to transcriptional activation of inflammatory or anti-inflammatory genes; the M2-polarized macrophage principally relies on OXPHOS and FAO, whereas the M1-polarized macrophage depends on glycolysis for energy production [45]. Our gene enrichment results showed that FAO and OXPHOS were significantly altered in M2 macrophages after CBD treatment (Fig. 3I). Therefore, we performed extracellular flux analysis. M2 polarization leads to an increase in the OCR, indicating a preference for OXPHOS (Fig. S8C). We found that CBD treatment reduced M2 polarization-induced increases in OCR (Figs. 7A, S8D, and S8E). Consistently, the extracellular acidification rate (ECAR) was significantly increased upon CBD treatment (Figs. 7B, S8F, and S8G), indicating a metabolic shift from OXPHOS toward glycolysis. In addition, we also measured the ATP production and malondialdehyde (MDA) level in M2-polarized macrophages, which reflect the intracellular level of OXPHOS and lipid oxidation, respectively. Compared with the controls upon IL-4 stimulation, the ATP and MDA production of cells treated with CBD significantly decreased and, surprisingly, CBD treatment profoundly increased lactate production (Figs. 7C–E). The differential gene expression analysis between the vehicle and CBD groups showed that the expressions of oxidative phosphorylation-related genes (*Ndufa6*, *Ndufs4*, *Uqcrb*, etc.) were significantly decreased in M2 macrophages after CBD treatment (Fig. 7F). These results further confirm that CBD treatment alters the metabolic profile of macrophages. In addition, as the raw material for FAO, the accumulation of intracellular lipids decreased after CBD treatment, indicating impaired FAO (Figs. 7G and S8H).

Based on our data, we demonstrated that CBD switched the metabolic predilection of the M2 macrophage from OXPHOS and FAO to glycolysis. This raises the question of how CBD regulates macrophage metabolism. PI3K-Akt-mTOR signaling regulates multiple metabolic pathways, including glycolysis, fatty acid synthesis, and protein synthesis in macrophages. Activated PI3K-Akt signaling has been recognized as an essential step toward alternative activation of macrophages [46–48]. Our scRNA-seq analysis of macrophages showed that mTORC1 signaling and PI3K-Akt signaling were significantly enriched between the vehicle and CBD treatment groups. Therefore, we detected the phosphorylation of PI3K and Akt under M2-polarization conditions, and the results showed that CBD profoundly inhibited the level of phosphorylated

PI3K (Tyr458) and Akt (Ser473) upon IL-4 stimulation (Figs. 7H, 7I, and S8I). Notably, the expression of genes related to PI3K-Akt signaling (*Akt1*, *Pi3kca*, and *Mapk1*) in macrophages was significantly reduced after CBD treatment (Fig. 7J). In addition, the expression of genes related to macrophage activation (*Myd88*) and antigen presentation (*H2-Aa* and *Cd74*) was significantly up-regulated after CBD treatment (Fig. S8J). Overall, our data suggest that CBD regulates the alternative activation of macrophages by PI3K-Akt signaling.

### 3.9. CBD synergizes with PD-1 blockade to suppress colon cancer progression

Considering the hindrance of M2 macrophages in monotherapy, we proceeded to explore the benefit of CBD on anti-PD-1 immunotherapy. Mice bearing MC38 tumors (~100 mm<sup>3</sup>) were randomly divided into four groups ( $n = 8$ ) and treated with vehicle, CBD, CBD and anti-PD-1 or anti-PD-1 alone. The results showed that mice treated with CBD and anti-PD-1 exhibited better anti-tumor effects than mice receiving either CBD or anti-PD-1 monotherapy (Figs. 8A–E and S9A). Moreover, CBD diminished M2 macrophages in the tumor while slightly increasing M1 macrophages (Figs. 8F and H). In addition, we observed a significant increase in the number of CD8<sup>+</sup> cells and GZMB<sup>+</sup> cells in the combination treatment group (Figs. 8G and S9B–D), and the expression of *Ifng* and *Tnf* genes was also enhanced (data not shown). In conclusion, our findings suggest that CBD inhibits alternative activation of macrophages and shifts the metabolic process from OXPHOS and FAO to glycolysis by inhibiting the PI3K-Akt signaling pathway. Furthermore, CBD-induced macrophage metabolic reprogramming restores their intrinsic anti-tumor ability, which synergizes with PD-1 blockade to inhibit tumor progression (Fig. 9).

## 4. Discussion

As cancer progresses, the TAMs in the TME adopt an immunosuppressive M2-like phenotype to support tumor growth [49]. Targeting the macrophage phenotype to de-suppress the TME may enhance the response to immunotherapy. Recent studies have found that macrophages in the TME could switch from the immunosuppressive phenotype to the anti-tumor phenotype [50,51]. It has been shown that, in addition to inducing tumor cell cycle arrest, paclitaxel skews TAMs toward the immune activity profile through Toll-like receptor 4 (TLR4), which might contribute to the anti-tumor effect of paclitaxel [52]. The TLR4 agonist monophosphoryl lipid A combined with IFN $\gamma$  reprograms CD206<sup>+</sup> TAMs to iNOS<sup>+</sup> macrophages to kill cancer cells and activate T cells to control metastatic breast cancer and ovarian cancer in mice [53]. These findings suggest that the state of macrophage polarization is important for the effective control of tumor progression, and that targeting macrophages to relieve the suppressive immune microenvironment may improve the efficacy of immunotherapy.

Previous research on CBD has focused on the nervous system as it is easy to pass through the blood-brain barrier. In addition, the anti-proliferative effects of CBD have long been explored to treat malignant tumors. Studies have shown that CBD could inhibit the proliferation of human glioma cells effectively both in vivo and in vitro. CBD could also inhibit tumor growth significantly in mouse

expression (inferred from scRNA-seq). (I) Genome track visualization of the *Stat1* locus (chr16:36,616,076–36,716,077). Inferred peak-to-gene links for distal regulatory elements are shown below. (J) Heatmap showing the positive TF regulators for which gene expression is positively correlated with TF deviation (inferred by chromVAR) across the M1-like macrophages cell trajectory. DCs: dendritic cells; TSS: transcriptional start site.

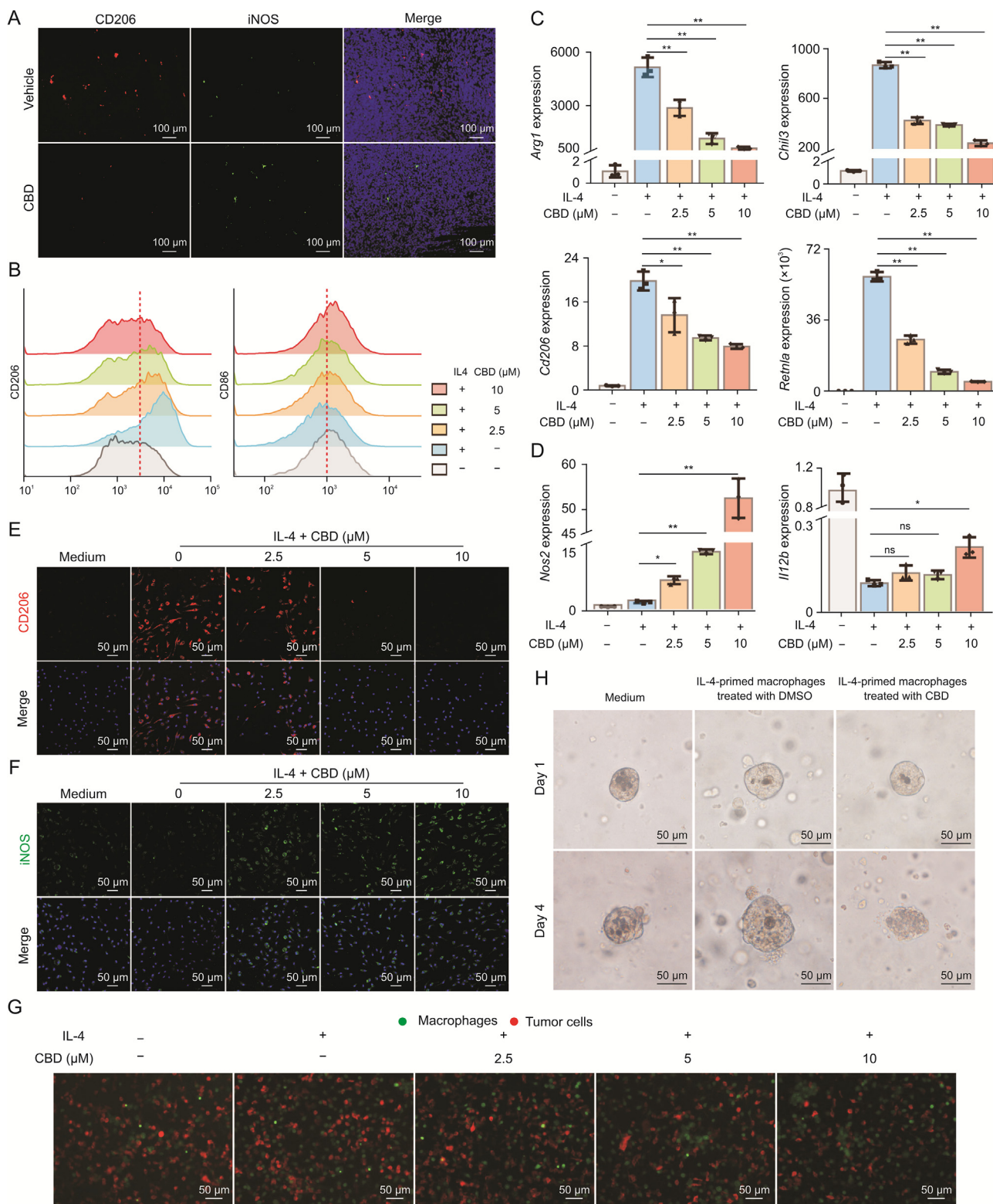


**Fig. 6.** Cannabidiol (CBD) suppresses alternative activation of macrophage in vitro. (A) Immunofluorescence staining of tumor tissue from vehicle or CBD treatment mice with CD206 and inducible NO synthase (iNOS). (B–D) Bone marrow-derived macrophages (BMDMs) were stimulated with media or interleukin-4 (IL-4) (20 ng/mL) then treated with dimethyl sulfoxide (DMSO) (vehicle control) or increasing concentrations ( $\mu$ M) of CBD for 24 h. (B) Flow cytometry data for the M2-specific surface marker CD206 (left) and M1 surface marker CD86 (right). (C) Quantitative real-time polymerase chain reaction (qRT-PCR) results showing mRNA expression of *Arg1*, *Cd206*, *Chil3*, and *Retnla* normalized to  $\beta$ -actin. (D) qRT-PCR results showing mRNA expression of *Il12b* and *Nos2* normalized to  $\beta$ -actin. (E, F) BMDMs were stimulated with medium or IL-4 and treated with DMSO or CBD for 24 h. Immunofluorescence images showing the expression of CD206 (E) and iNOS (F). (G) BMDMs were stimulated with medium or IL-4 (20 ng/mL) and treated with DMSO or CBD for 24 h then co-cultured with MC38-mCherry cells for another 48 h. (H) Time course images of organoid on day 1 and day 4 ( $n = 6–8$  for each time point). Data are represented as mean  $\pm$  standard error of mean. \* $P < 0.05$  and \*\* $P < 0.01$ . ns: no significance.

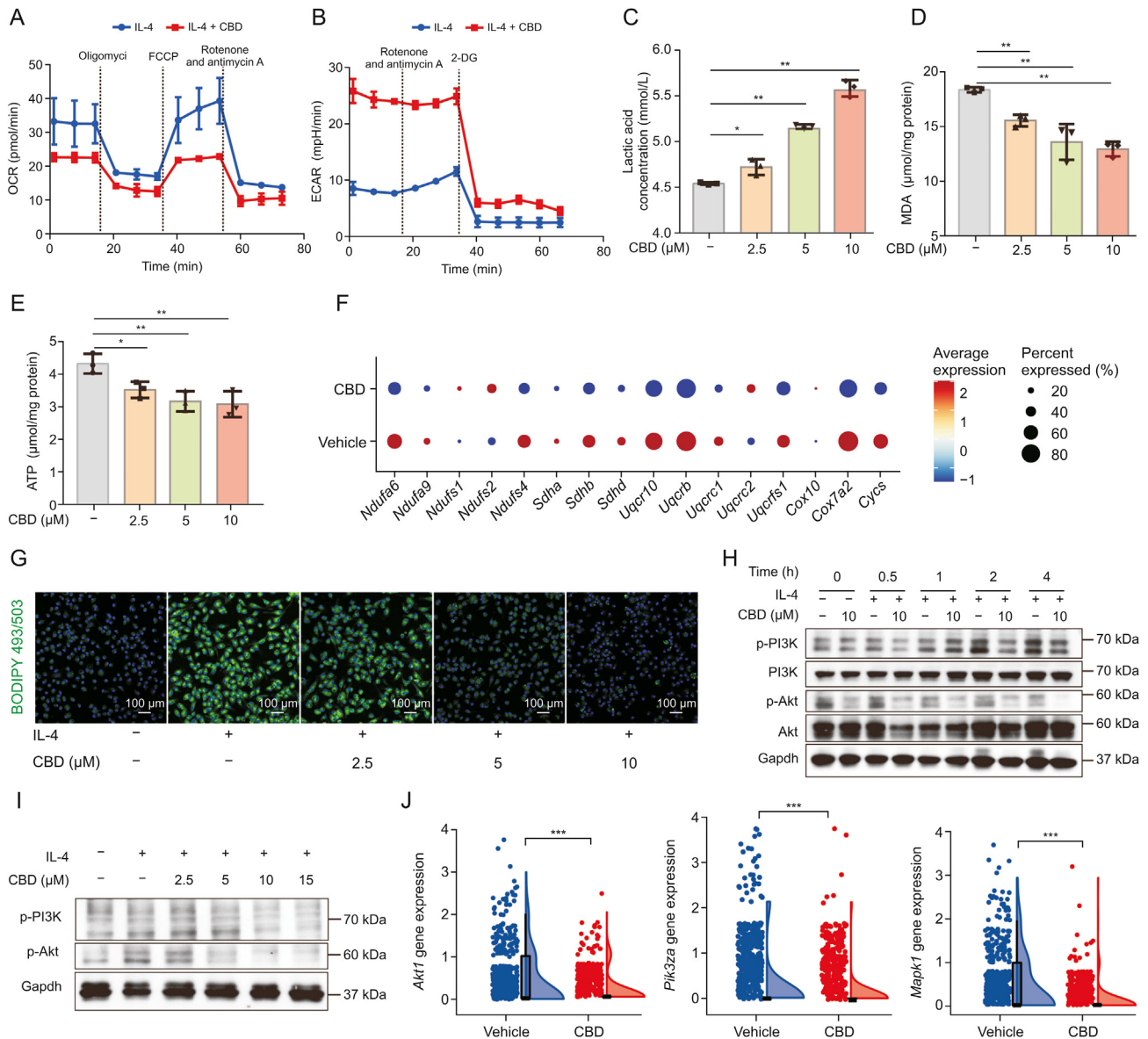


**Fig. 7.** Cannabidiol (CBD) regulates macrophage polarization by inhibiting phosphatidylinositol 3-kinase (PI3K)/protein kinase B (Akt) signaling. (A) Oxygen consumption rate (OCR) and (B) extracellular acidification rate (ECAR) of interleukin-4 (IL-4)-primed bone marrow-derived macrophages (BMDMs) treated with dimethyl sulfoxide (DMSO) or CBD for 24 h. (C–E) BMDMs were stimulated with media or IL-4 (20 ng/mL) then treated with DMSO (vehicle control) or increasing concentrations (μM) of CBD for 24 h. (C) Lactic acid content, (D) malondialdehyde (MDA) content, and (E) adenosine triphosphate (ATP) production in polarized macrophage. (F) Bubble plot showing the expressions of oxidative phosphorylation-related genes from vehicle and CBD groups. (G) BMDMs grown on coverslips treated with media or IL-4 with or without CBD. The cells were analyzed according to the section titled ‘BODIPY’ staining for microscopy. (H, I) BMDMs cells were pretreated with DMSO or increasing concentrations of CBD for 2 h and then stimulated with media or IL-4 for the indicated time. The protein levels of p-PI3K, PI3K, p-Akt, and Akt were analyzed by Western blot. β-Actin is shown as a loading control. (J) Raincloud plots show the expression of glycolysis and lipid metabolism gene in macrophages. Data are represented as mean ± standard error of mean. \**P* < 0.05, \*\**P* < 0.01, and \*\*\**P* < 0.001. FCCP: fluoro-carbonyl cyanide phenylhydrazine; 2-DG: 2-deoxy-D-glucose; Gapdh: glyceraldehyde-3-phosphate dehydrogenase.

orthotopic models, while further mechanism studies have shown that CBD can induce autophagy and cause tumor cell death [21,54]. It has also been revealed that CBD can not only inhibit ERK signaling in human glioma cells, but also inhibit the expression of hypoxia-inducible factor HIF1α, thereby dually inhibiting tumor proliferation as well as tumor angiogenesis [55]. In addition to its role in nervous system tumors, many studies have reported the anti-tumor effect of CBD on colorectal cancer. Increasing evidence has shown that CBD activates ROS production in colorectal cancer cells, causing mitochondrial dysfunction and cell death [56]. Moreover, CBD may be used as an adjuvant to chemotherapy in treating colorectal cancer, and the combination of CBD with chemotherapy drugs such as 5-Fu and oxaliplatin may enhance its anti-tumor

effect [57]. Despite the impacts on the tumor cells, whether CBD would inhibit tumor progression through remodeling TME remains unclear. Our study provided a new insight that CBD would exert anti-tumor effects, at least in part by modulating immune responses.

Single-cell transcriptome sequencing, as a rapidly developing frontier technology in life sciences, has dramatically advanced disease research [58,59]. Here, using single-cell transcriptome sequencing technology, we detected cellular components in the TME after CBD treatment and found that CBD significantly altered the number and proportion of myeloid cells in the TME. It is well known that myeloid cells play a critical role in tumor progression. Further, we divided myeloid cells into five populations, including

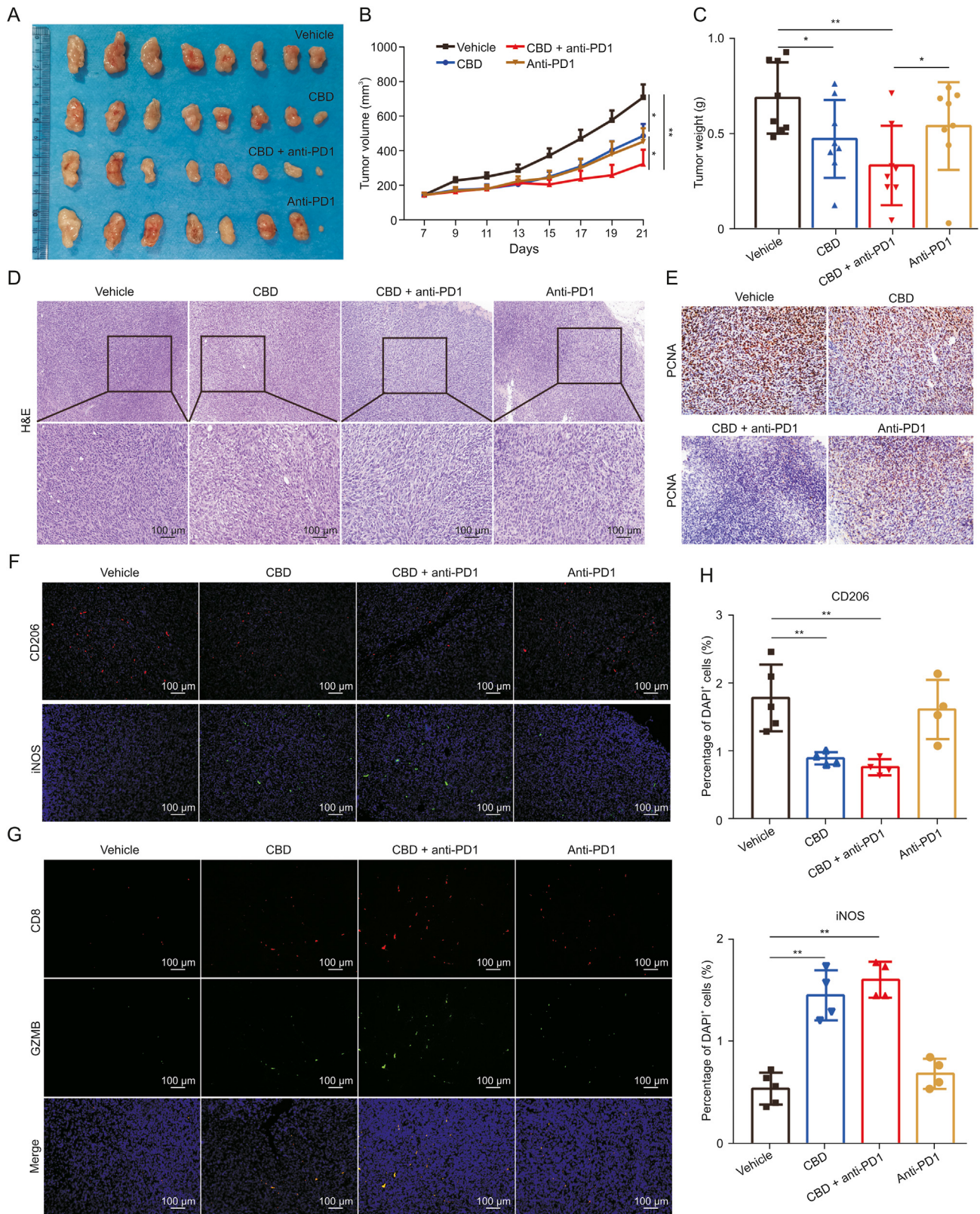


**Fig. 8.** The combination of cannabidiol (CBD) and programmed cell death protein 1 (PD-1) antibody shows stronger anti-tumor effect. (A–C) Effects of CBD and anti-PD-1 on tumor growth. (B) Tumor volume and (C) tumor weight of MC38-derived tumors in the subcutaneous C57BL/6 mouse model. (D) Hematoxylin & eosin (H&E) and (E) proliferating cell nuclear antigen (PCNA) staining of tumor sections. Representative immunofluorescent staining for M1 cells (inducible NO synthase (iNOS)) and (F) M2 cells (CD206) and (G) CD8<sup>+</sup> T cells in tumor. (H) Percentage of CD206 and iNOS positive cells in panel. Data are represented as mean ± standard error of mean. \**P* < 0.05 and \*\**P* < 0.01. DAPI: 4'-6-diamidino-2-phenylindole; GZMB: granzyme B.

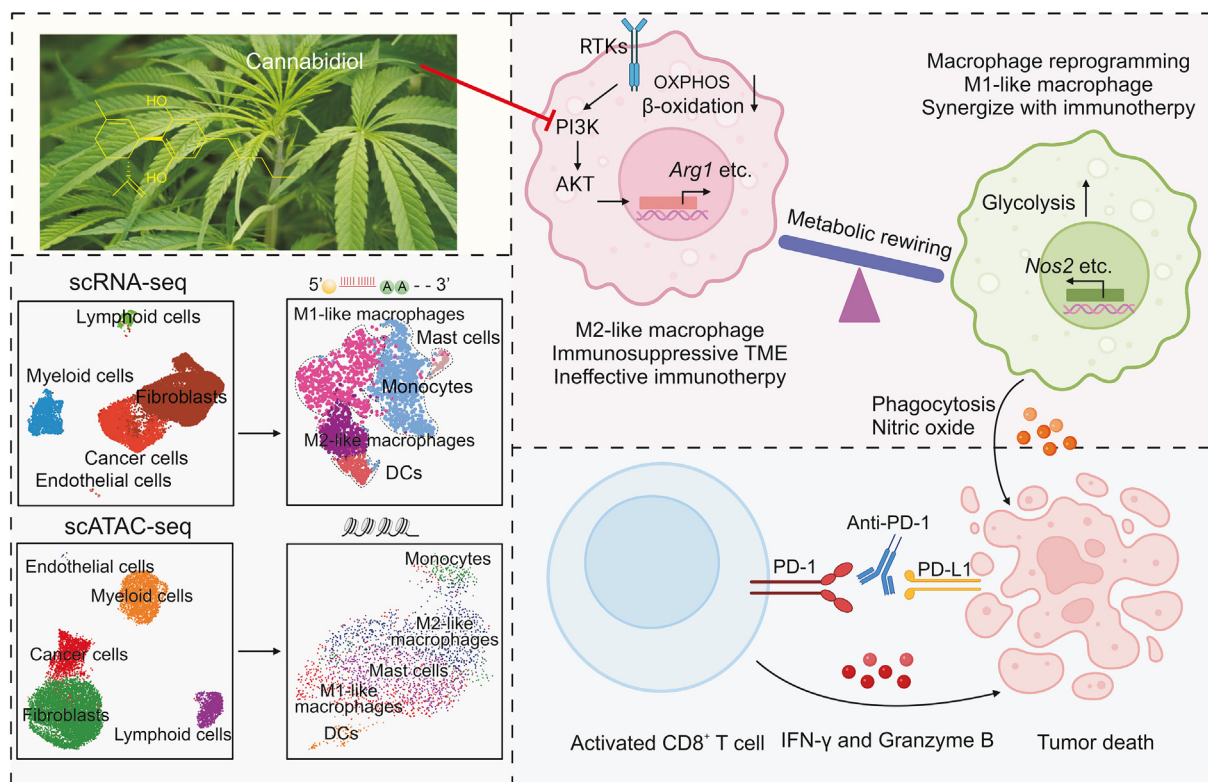


**Fig. 9.** Graphic illustration of the anti-tumor mechanism of cannabidiol (CBD) in colon cancer. The tumor microenvironment (TME) of all cell types in mouse MC38 xenograft tumors after CBD treatment was investigated by single-cell RNA sequencing (scRNA-seq) and single-cell ATAC sequencing (scATAC-seq). CBD inhibits the alternative activation of macrophages and shifts the metabolic process from oxidative phosphorylation and fatty acid oxidation to glycolysis by inhibiting the phosphatidylinositol 3-kinase (PI3K)-protein kinase B (Akt) signaling pathway and related downstream target genes, which relieves the inhibitory immune microenvironment and restores the intrinsic anti-tumor effects of macrophages. Furthermore, CBD-mediated macrophage plasticity enhances the response to anti-programmed cell death protein 1 (PD-1) immunotherapy in xenografted mice. OXPHOS: oxidative phosphorylation; DCs: dendritic cells; RTKs: receptor protein tyrosine kinases; IFN- $\gamma$ : interferon-gamma.

classically activated M1 and alternatively activated M2 macrophages. CBD significantly decreased the number of M2 macrophages and, correspondingly, the number of M1 macrophages was increased, which significantly promoted anti-tumor immunity. This result was further confirmed by immunofluorescence staining. Accordingly, we hypothesized that CBD may affect the alternative activation of macrophages in the tumor microenvironment and therefore examined the effect of CBD on macrophage polarization in vitro. CBD was found to inhibit IL-4-induced expression of anti-inflammatory genes, which was largely dependent on the inhibitory effect of CBD on PI3K-Akt signaling. Macrophage activation involves extensive metabolic reprogramming, glycolytic switching, and phospholipid remodeling. Recent studies have shown macrophage polarization signals affect metabolic signaling pathways [16,60]. As a metabolic regulatory signal, mTOR-PI3K has been identified as a key regulator of the macrophage switch between immune stimulation and suppression [46,48]. This is consistent with our research that CBD indeed affects the metabolic shift of macrophages. Under IL-4-induced anti-inflammatory polarization conditions, CBD inhibited oxidative phosphorylation and fatty acid oxidation levels while promoting glycolysis in macrophages. Most importantly, CBD treatment substantially enhanced the efficacy of immune checkpoint inhibitor anti-PD-1 in a mouse model (Fig. 8). Consistent with previous results, CBD decreased the number of pro-tumor macrophages and increased the number of anti-tumor macrophages in tumors. These findings suggest that CBD rewires TME through inhibiting the alternative activation of macrophages, resulting in the inhibition of tumor-bearing mice.

Studies have reported that THC could impair the function of

tumor-specific T cells through cannabinoid receptor 2, and thereby, reduce the therapeutic effect of PD-1 blockade [61]. We did not observe such results with CBD in vitro. Consequently, further research focusing on the regulation of CBD on the anti-tumor immune system is needed. Clarification regarding the specific targets of CBD regulating macrophages should also be conducted. To sum up, this study demonstrated that CBD inhibits the alternative activation of macrophages to modulate the suppressive tumor immune microenvironment and improves the therapeutic outcome of cancer immune therapies (Fig. 9). Our study provides new insights into the anti-tumor effects of CBD, which might be a theoretical basis for the future application of cannabinoids in the anti-tumor market.

## 5. Conclusion

We investigated the TME in mouse MC38 xenograft tumors after CBD treatment by scRNA-seq and scATAC-seq. It was found that by inhibiting the PI3K-Akt signaling pathway and related downstream target genes, CBD shifts the metabolic process from oxidative phosphorylation and fatty acid oxidation to glycolysis and inhibits the alternative activation of macrophages, thereby restoring the intrinsic antitumor effects of macrophages. Furthermore, CBD-mediated macrophage plasticity enhanced the response of xenografted mice to anti-PD1 immunotherapy.

## CRedit author statement

**Xiaofan Sun:** Data curation, Investigation, Methodology, Validation, Writing - Original draft preparation, Reviewing and Editing,

Visualization; **Lisha Zhou**: Data curation, Visualization, Validation, Writing - Original draft preparation, Reviewing and Editing; **Yi Wang**: Data curation, Visualization, Validation; **Guoliang Deng**: Data curation, Investigation, Methodology, Validation, Visualization; **Xinran Cao**: Data curation, Writing - Original draft preparation, Reviewing and Editing; **Bowen Ke**: Resources, Formal analysis, Suggestions; **Xiaoqi Wu**: Data curation, Visualization, Validation; **Yanhong Gu, Haibo Cheng, and Qiang Xu**: Resources, Formal analysis, Suggestions; **Qianming Du**: Methodology, Conceptualization, Formal analysis, Project administration; **Hongqi Chen**: Methodology, Conceptualization, Formal analysis, Project administration; **Yang Sun**: Methodology, Conceptualization, Formal analysis, Visualization, Writing - Original draft preparation, Reviewing and Editing, Resources, Funding acquisition, Project administration, Supervision.

### Declaration of competing interest

The authors declare that there are no conflicts of interests.

### Acknowledgments

This work was supported by the National Key Research and Development Plan, China (Grant No.: 2022YFC3500202), the Natural Science Foundation of China (Grant Nos.: 82172558, and 82205024), the Scientific and Technological Innovation Action Plan of Natural Science Foundation Project of Shanghai, China (Grant No.: 22ZR1447400), the Scientific and Technological Innovation Action Plan, China (Grant No.: 22ZR1447400), the Fundamental Research Funds for the Central Universities, China (Grant Nos.: 020814380179, and 020814380174), the Distinguished Young Scholars of Nanjing, China (Grant No.: JQX20008), and the School of Life Science (NJU)-Sipimo Joint Funds and Mountain Climbing Talents Project of Nanjing University, China (Grant No.: 2015018).

### Appendix A. Supplementary data

Supplementary data to this article can be found online at <https://doi.org/10.1016/j.jpha.2023.04.013>.

### References

- [1] F. Ciardiello, D. Ciardiello, G. Martini, et al., Clinical management of metastatic colorectal cancer in the era of precision medicine, *CA Cancer J. Clin.* 72 (2022) 372–401.
- [2] R.L. Siegel, K.D. Miller, A. Goding Sauer, et al., Colorectal cancer statistics, 2020, *CA Cancer J. Clin.* 70 (2020) 145–164.
- [3] K. Ganesh, Z.K. Stadler, A. Cercek, et al., Immunotherapy in colorectal cancer: Rationale, challenges and potential, *Nat. Rev. Gastroenterol. Hepatol.* 16 (2019) 361–375.
- [4] K. Ganesh, Optimizing immunotherapy for colorectal cancer, *Nat. Rev. Gastroenterol. Hepatol.* 19 (2022) 93–94.
- [5] S.P. Kubli, T. Berger, D.V. Araujo, et al., Beyond immune checkpoint blockade: Emerging immunological strategies, *Nat. Rev. Drug Discov.* 20 (2021) 899–919.
- [6] M. Schmitt, F.R. Greten, The inflammatory pathogenesis of colorectal cancer, *Nat. Rev. Immunol.* 21 (2021) 653–667.
- [7] Y. Tie, F. Tang, Y.Q. Wei, et al., Immunosuppressive cells in cancer: Mechanisms and potential therapeutic targets, *J. Hematol. Oncol.* 15 (2022), 61.
- [8] D.G. DeNardo, B. Ruffell, Macrophages as regulators of tumour immunity and immunotherapy, *Nat. Rev. Immunol.* 19 (2019) 369–382.
- [9] A. Mantovani, P. Allavena, F. Marchesi, et al., Macrophages as tools and targets in cancer therapy, *Nat. Rev. Drug Discov.* 21 (2022) 799–820.
- [10] X. Xiang, J. Wang, D. Lu, et al., Targeting tumor-associated macrophages to synergize tumor immunotherapy, *Signal Transduct. Target. Ther.* 6 (2021), 75.
- [11] P.J. Murray, J.E. Allen, S.K. Biswas, et al., Macrophage activation and polarization: Nomenclature and experimental guidelines, *Immunity* 41 (2014) 14–20.
- [12] R. Stienstra, R.T. Netea-Maier, N.P. Riksen, et al., Specific and complex reprogramming of cellular metabolism in myeloid cells during innate immune responses, *Cell Metabol.* 26 (2017) 142–156.
- [13] J. Van den Bossche, L.A. O'Neill, D. Menon, Macrophage immunometabolism: Where are we (going)? *Trends Immunol.* 38 (2017) 395–406.
- [14] M. Zhang, X. Pan, K. Fujiwara, et al., Pancreatic cancer cells render tumor-associated macrophages metabolically reprogrammed by a GARP and DNA methylation-mediated mechanism, *Signal Transduct. Target. Ther.* 6 (2021) 366.
- [15] J.L. Wilson, T. Weichhart, TORChing a semaphore for alternative macrophage activation, *Nat. Immunol.* 19 (2018) 512–514.
- [16] S. Kang, Y. Nakanishi, Y. Kioi, et al., Semaphorin 6D reverse signaling controls macrophage lipid metabolism and anti-inflammatory polarization, *Nat. Immunol.* 19 (2018) 561–570.
- [17] R. Dash, M.C. Ali, I. Jahan, et al., Emerging potential of cannabidiol in reversing proteinopathies, *Ageing Res. Rev.* 65 (2021), 101209.
- [18] P. Grimison, A. Mersiades, A. Kirby, et al., Oral THC:CBD cannabis extract for refractory chemotherapy-induced nausea and vomiting: A randomised, placebo-controlled, phase II crossover trial, *Ann. Oncol.* 31 (2020) 1553–1560.
- [19] A. Oláh, B.I. Tóth, I. Borbíró, et al., Cannabidiol exerts sebostatic and anti-inflammatory effects on human sebocytes, *J. Clin. Invest.* 124 (2014) 3713–3724.
- [20] M. Rajesh, P. Mukhopadhyay, S. Batakai, et al., Cannabidiol attenuates cardiac dysfunction, oxidative stress, fibrosis, and inflammatory and cell death signaling pathways in diabetic cardiomyopathy, *J. Am. Coll. Cardiol.* 56 (2010) 2115–2125.
- [21] T. Huang, T. Xu, Y. Wang, et al., Cannabidiol inhibits human glioma by induction of lethal mitophagy through activating TRPV4, *Autophagy* 17 (2021) 3592–3606.
- [22] A. Shrivastava, P.M. Kuzontkoski, J.E. Groopman, et al., Cannabidiol induces programmed cell death in breast cancer cells by coordinating the cross-talk between apoptosis and autophagy, *Mol. Cancer Ther.* 10 (2011) 1161–1172.
- [23] B. Kis, F.C. Ifrim, V. Buda, et al., Cannabidiol-from plant to human body: A promising bioactive molecule with multi-target effects in cancer, *Int. J. Mol. Sci.* 20 (2019), 5905.
- [24] L. Lyon, THC and CBD: Is medical cannabis overhyped or under-prescribed? *Brain* 143 (2020), e34.
- [25] S.C. Britch, S. Babalonis, S.L. Walsh, Cannabidiol: Pharmacology and therapeutic targets, *Psychopharmacology (Berl.)* 238 (2021) 9–28.
- [26] E. Driehuis, K. Kretzschmar, H. Clevers, Establishment of patient-derived cancer organoids for drug-screening applications, *Nat. Protoc.* 15 (2020) 3380–3409.
- [27] A. Butler, P. Hoffman, P. Smibert, et al., Integrating single-cell transcriptomic data across different conditions, technologies, and species, *Nat. Biotechnol.* 36 (2018) 411–420.
- [28] G. Yu, L.G. Wang, Y. Han, et al., clusterProfiler: An R package for comparing biological themes among gene clusters, *OMICS* 16 (2012) 284–287.
- [29] T. Stuart, A. Butler, P. Hoffman, et al., Comprehensive integration of single-cell data, *Cell* 177 (2019) 1888–1902.e21.
- [30] J.M. Granja, M.R. Corces, S.E. Pierce, et al., ArchR is a scalable software package for integrative single-cell chromatin accessibility analysis, *Nat. Genet.* 53 (2021) 403–411.
- [31] I. Korsunsky, N. Millard, J. Fan, et al., Fast, sensitive and accurate integration of single-cell data with Harmony, *Nat. Methods* 16 (2019) 1289–1296.
- [32] D. van Dijk, R. Sharma, J. Nainys, et al., Recovering gene interactions from single-cell data using data diffusion, *Cell* 174 (2018) 716–729.e27.
- [33] Y. Zhang, T. Liu, C.A. Meyer, et al., Model-based analysis of ChIP-seq (MACS), *Genome Biol.* 9 (2008), R137.
- [34] C. Trapnell, D. Cacchiarelli, J. Grimsby, et al., The dynamics and regulators of cell fate decisions are revealed by pseudotemporal ordering of single cells, *Nat. Biotechnol.* 32 (2014) 381–386.
- [35] X. Qiu, A. Hill, J. Packer, et al., Single-cell mRNA quantification and differential analysis with Census, *Nat. Methods* 14 (2017) 309–315.
- [36] X. Qiu, Q. Mao, Y. Tang, et al., Reversed graph embedding resolves complex single-cell trajectories, *Nat. Methods* 14 (2017) 979–982.
- [37] A. Subramanian, P. Tamayo, V.K. Mootha, et al., Gene set enrichment analysis: A knowledge-based approach for interpreting genome-wide expression profiles, *Proc. Natl. Acad. Sci. U S A* 102 (2005) 15545–15550.
- [38] S. Hänzelmann, R. Castelo, J. Guinney, GSEA: Gene set variation analysis for microarray and RNA-seq data, *BMC Bioinformatics* 14 (2013), 7.
- [39] S. Jin, C.F. Guerrero-Juarez, L. Zhang, et al., Inference and analysis of cell-cell communication using CellChat, *Nat. Commun.* 12 (2021), 1088.
- [40] Y.J. Li, C. Zhang, A. Martincuks, et al., STAT proteins in cancer: Orchestration of metabolism, *Nat. Rev. Cancer* 23 (2023) 115–134.
- [41] A. Kauppinen, T. Suuronen, J. Ojala, et al., Antagonistic crosstalk between NF- $\kappa$ B and SIRT1 in the regulation of inflammation and metabolic disorders, *Cell. Signal.* 25 (2013) 1939–1948.
- [42] J. Qi, H. Sun, Y. Zhang, et al., Single-cell and spatial analysis reveal interaction of FAP<sup>+</sup> fibroblasts and SPP1<sup>+</sup> macrophages in colorectal cancer, *Nat. Commun.* 13 (2022), 1742.
- [43] M. Faas, N. Ipseiz, J. Ackermann, et al., IL-33-induced metabolic reprogramming controls the differentiation of alternatively activated macrophages and the resolution of inflammation, *Immunity* 54 (2021) 2531–2546.e5.
- [44] S.Y. Weng, X. Wang, S. Vijayan, et al., IL-4 receptor alpha signaling through macrophages differentially regulates liver fibrosis progression and reversal, *EBioMedicine* 29 (2018) 92–103.
- [45] K. Mehla, P.K. Singh, Metabolic regulation of macrophage polarization in cancer, *Trends Cancer* 5 (2019) 822–834.
- [46] M.M. Kaneda, K.S. Messer, N. Ralainirina, et al., PI3K $\gamma$  is a molecular switch that controls immune suppression, *Nature* 539 (2016) 437–442.

- [47] E. Vergadi, E. Ieronymaki, K. Lyroni, et al., Akt signaling pathway in macrophage activation and M1/M2 polarization, *J. Immunol.* 198 (2017) 1006–1014.
- [48] A.J. Covarrubias, H.I. Aksoylar, J. Yu, et al., Akt-mTORC1 signaling regulates Acly to integrate metabolic input to control of macrophage activation, *eLife* 5 (2016), 11612.
- [49] X. Li, R. Liu, X. Su, et al., Harnessing tumor-associated macrophages as aids for cancer immunotherapy, *Mol. Cancer* 18 (2019), 177.
- [50] H.M. Chen, W. van der Touw, Y.S. Wang, et al., Blocking immunoinhibitory receptor LILRB2 reprograms tumor-associated myeloid cells and promotes antitumor immunity, *J. Clin. Invest.* 128 (2018) 5647–5662.
- [51] A.N. Chamseddine, T. Assi, O. Mir, et al., Modulating tumor-associated macrophages to enhance the efficacy of immune checkpoint inhibitors: A TAM-priming approach, *Pharmacol. Ther.* 231 (2022), 107986.
- [52] C.W. Wanderley, D.F. Colón, J.P.M. Luiz, et al., Paclitaxel reduces tumor growth by reprogramming tumor-associated macrophages to an M1 profile in a TLR4-dependent manner, *Cancer Res.* 78 (2018) 5891–5900.
- [53] L. Sun, T. Kees, A.S. Almeida, et al., Activating a collaborative innate-adaptive immune response to control metastasis, *Cancer Cell* 39 (2021) 1361–1374.e9.
- [54] C. Gross, D.A. Ramirez, S. McGrath, et al., Cannabidiol induces apoptosis and perturbs mitochondrial function in human and canine glioma cells, *Front. Pharmacol.* 12 (2021), 725136.
- [55] P. Massi, A. Vaccani, S. Ceruti, et al., Antitumor effects of cannabidiol, a non-psychoactive cannabinoid, on human glioma cell lines, *J. Pharmacol. Exp. Ther.* 308 (2004) 838–845.
- [56] S. Jeong, H.K. Yun, Y.A. Jeong, et al., Cannabidiol-induced apoptosis is mediated by activation of Noxa in human colorectal cancer cells, *Cancer Lett.* 447 (2019) 12–23.
- [57] S. Jeong, B.G. Kim, D.Y. Kim, et al., Cannabidiol overcomes oxaliplatin resistance by enhancing NOS3- and SOD2-induced autophagy in human colorectal cancer cells, *Cancers (Basel)* 11 (2019), 781.
- [58] Y. Zhu, Z. Ouyang, H. Du, et al., New opportunities and challenges of natural products research: When target identification meets single-cell multiomics, *Acta Pharm. Sin. B* 12 (2022) 4011–4039.
- [59] G. Deng, L. Zhou, B. Wang, et al., Targeting cathepsin B by cycloastragenol enhances antitumor immunity of CD8 T cells via inhibiting MHC-I degradation, *J. Immunother. Cancer* 10 (2022), e004874.
- [60] E. Sanchez-Lopez, Z. Zhong, A. Stubelius, et al., Choline uptake and metabolism modulate macrophage IL-1 $\beta$  and IL-18 production, *Cell Metab.* 29 (2019) 1350–1362.e7.
- [61] X. Xiong, S. Chen, J. Shen, et al., Cannabis suppresses antitumor immunity by inhibiting JAK/STAT signaling in T cells through CNR2, *Signal Transduct. Targeted Ther.* 7 (2022), 99.